$$l_{stride} = l_{thigh}\sin(\theta_{abs}-\theta_{hr}) + l_{shank}\sin(\theta_{kr}+\theta_{abs}-\theta_{hr}) - l_{thigh}\sin(\theta_{abs}-\theta_{hl}) - l_{shank}\sin(\theta_{kl}+\theta_{abs}-\theta_{hl}) \quad (6)$$

where l_{stride} is a defined stride.

Fig. 5 shows the coordinate system of CoGRF when legs are placed back and forth. This coordinate system is different from the coordinate system shown in Fig. 2. That is, the representative FRF measuring point of a toe of the back side leg, and representative FRF measuring point of a heel of the forth side leg are placed at different points from the points on the coordinate system shown in Fig. 2. In that coordinate system, CoGRF in sagittal plane is calculated as follows.

$$C'_y = \begin{cases} \dfrac{|l_{stride}|C_x + l_{sole}C_y}{|l_{stride}| + l_{sole}} & (l_{stride} \geq 0) \\ \dfrac{|l_{stride}|(1-C_x) + l_{sole}C_y}{|l_{stride}| + l_{sole}} & (l_{stride} < 0) \end{cases} \quad (7)$$

where C'_y is CoGRF in sagittal plane when legs are placed back and forth; l_{sole} is the length of the sole which is defined as the distance between representative FRF measuring points of heel and toe in the same sole.

In the sagittal plane, the threshold which determines whether CoGRF is in the single leg stance leg polygon or not is defined as follows.

$$C'_y > \frac{|l_{stride}|}{l_{sole} + |l_{stride}|} \quad (8)$$

Proposed phase determination for stair ascent uses (8), and the threshold of CoGRF in lateral plane that is the same as walking assistance. Fig. 6 shows the follow chart of the phase determination. The phase determination determines three phases in stair ascent, that is, $L_{st}R_{sw}$, D_{st} and $L_{sw}R_{st}$. When the height of landing area is lower than the height of a step, the determination determines that wearer is walking.

III. Automatic Control For Stair Ascent Assistance

In stair ascent, movements of wearer are different between phases. In swing phase, joints of the swing leg are flexed voluntarily to land the foot on the upper step. In double stance phase, joints of the leg on the lower step are extended to keep the leg in extended position for weight bearing, and joints of the leg on the upper step are flexed to move the CoGRF into the stance leg polygon of upper leg. In single stance phase, the hip joint is rotated to keep the CoGRF in the supporting leg polygon, and the knee joint is extended to lift up the body [6].

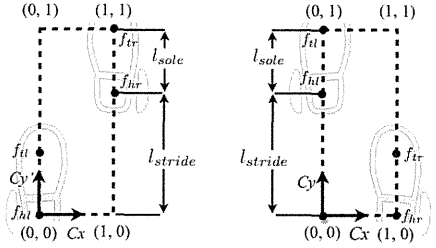

Fig. 5. The coordinate system of CoGRF when legs are placed back and forth. When left leg is forth (Left). When right leg is forth (Right). This coordinate system is different from the coordinate system shown in Fig. 2. That is, the representative FRF measuring point of a toe of the back side leg, and representative FRF measuring point of a heel of the forth side leg are placed at different points from the points on the coordinate system shown in Fig. 2.

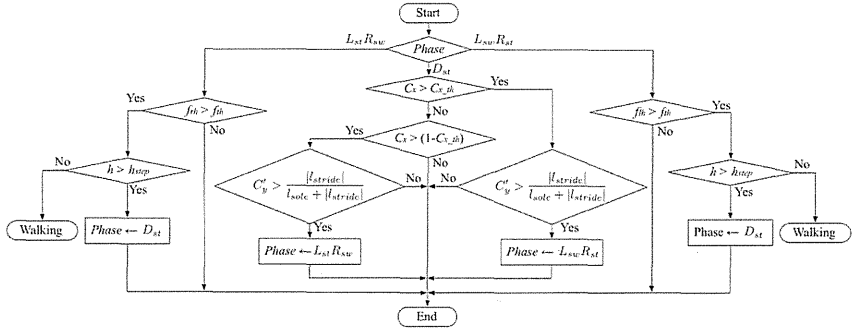

Fig. 6. The follow chart of the phase determination for stair ascent. Where h_{step} is the predefined height of a step; "Walking" means the control method is switched into walking assistance.

We propose an automatic control method for assisting stair ascent, which is based on the movement of each phase. The method consists of three algorithms: gravity compensation in the swing phase, assistance of weight bearing in the double stance phase and assistance of upward movement in the single stance phase.

The movement of swing leg and the movement of stance leg on the lower step are the same as in walking. Thus, gravity compensation and assistance of weight bearing proposed in previous study could be used for these movements. In this method, we propose an automatic control for assisting upward movement in the single stance phase.

When wearer moves upward, a following load is applied to the knee joint

$$W = \begin{cases} (1-C_x)M & (Phase = L_{st}R_{sw}) \\ C_x M & (Phase = L_{sw}R_{st}) \end{cases} \quad (9)$$

where W is applied load to the knee joint; M is the weight of the wearer.

To lift wearer's body up, flowing knee joint torque is generated.

$$\tau_k = Wgl \quad (10)$$

where τ_k is generated knee joint torque; g is acceleration of gravity; l is distance between knee joint and center of gravity (COG) in sagittal plane.

As shown in Fig. 7, the force vector from the COG and the force vector from the CoGRF are placed at the same point [7].

Thus, in single stance phase, l is defined as distance between CoGRF in sagittal plane and knee joint.

In that case, knee joint torque τ_k is calculated as

$$\tau_k = Wg\{l_{shank}\sin(\theta_k + \theta_{abs} - \theta_h) - (l_{sole} + |l_{stride}|)C'_y + |l_{stride}|\} \quad (11)$$

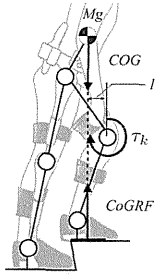

Fig. 7. The force vector from the COG and the force vector from CoGRF during moving upward. These vectors is considered to be in the same distance from the knee joint in the sagittal plane.

Proposed assistance of upward movement generates knee joint torque as follows.

$$\tau_{up} = G_{up}\tau_k \quad (12)$$

where τ_{up} is automatic generated torque for an upward movement assistance, G_{up} is the gain that adjusts the torque based on the body function of wearer.

IV. Experiments

An automatic control of the HAL for stair ascent assistance based on the proposed method was verified by experiments on flat area and stairs. Fig. 8 shows the environment of experiment. A step of the stair was 12 [cm] high, 72 [cm] wide, and a depth of 27 [cm].

The subject is a healthy male, 65 [kg] in weight, 166 [cm] in height, and the shoes size is 27 [cm]. The subject started walking voluntarily from 1.5 [m] away from the stairs. When arrived in front of the stairs, the subject started stair ascent. By this experiment, the validity of following three methods is examined.

A. Phase determination based on height of landing areas

The subject moved over flat area during walking and climbed up stairs during stair ascent. The proposed method was verified by comparing the heights of landing areas between walking and stair ascent. The Comparison is done by determining the significance difference using t-test. The heights were defined as the calculated height by using (2) at the moment of the phase was transited from a single stance phase to double stance phase.

B. CoGRF-based Phase determination

The phase was transited from double stance phase to single stance phase when CoGRF was in the stance leg polygon of the next single stance leg. The proposed method was verified by tracking the trajectory of CoGRF during the experiments. The trajectory was calculated based on the landed area of a stance leg.

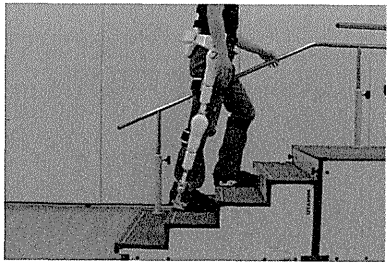

Fig. 8. Environment of experiment. The stair was used for rehabilitation training. For the safety of the subject, touching the handrail was allowed. Though, using the handrail to move upward was not allowed.

A landed area of stance leg was defined as the position at the moment when the phase was transited from a single stance phase to double stance phase. It is the same value as the distance from the starting point of the movement. And

can be obtained by integrating absolute value of l_{stride}.

C. Automatic Control For Stair Ascent Assistance

The proposed automatic control generated torque for assisting movement of each phase. The effectiveness is examined by measuring the transition between calculated torque (8) and commanded torque.

V. Result

A. Phase determination based on height of landing areas

We verified the phase determination. Fig. 9 shows transition of *h* during the experiment. Points in Fig. 9 shows the heights of landing areas. Table 1 shows mean values and valiances of the heights of landing areas during walking and stair ascent. P-value is calculated by t-test. The heights of landing areas during stair ascent are significantly higher than during walking.

B. CoGRF-based Phase determination

We verified the phase determination. Fig. 10 shows landed areas and the trajectory of CoGRF with time from 17.5 [s] to 19.5 [s]. Dashed lines show the thresholds to determine the phase based on CoGRF. Boxed areas in Fig. 10 shows the areas, that is, phase determination based on only CoGRF in lateral plane could not determine the correct phase. The trajectory of CoGRF was gone through the area.

C. Automatic Control For Stair Ascent Assistance

We verified the validity of assist torque. Fig. 11 shows transition of the generated torque and the calculated torque by (8) of right knee joint with time from 17.5 [s] to 19.5 [s]. During assisting upward movement, maximum commanded extension torque was measured. That was 39.4 [Nm]. The proposed method switched the upward movement assistance to the weight-bearing assistance when required torque for upward movement assistance was less than limited torque for weight-bearing assistance.

VI. Discussion

A range of activity is considered to be closely related to activity of daily living ability levels [8].

As a result of experiment, we verified that our proposed method generated appropriately assist for each movement phases. It indicates that, the method is applicable for walking and stair ascent assistance.

TABLE 1
MEAN VALUES AND VALIANCES OF THE HEIGHTS OF LANDING AREAS

Walking	Stair ascent	P-value
0.0440±0.012	0.122±0.006	$p < 0.001$

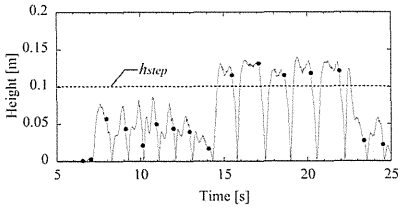

Fig. 9. Transition of *h* during the experiment. Points in the figure show the heights of landing areas. The heights of landing areas during stair ascent are significantly higher than during walking.

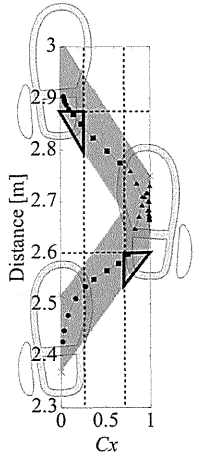

Fig. 10. Landing areas and the trajectory of CoGRF with time from 17.5 [s] to 19.5 [s]. Circle points show the CoGRF during $L_{st}R_{sw}$, rectangle points show the CoGRF during D_{st} and triangle points show the CoGRF during $L_{sw}R_{st}$. The gray area shows the defined stance leg polygon. Boxed areas shows the areas, that is, phase determination based on only CoGRF in lateral plane could not determine the correctly phase. Dashed lines show the threshold to determine the phase based on CoGRF.

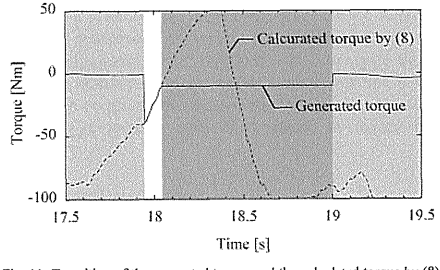

Fig. 11. Transition of the generated torque and the calculated torque by (8) of right knee joint with time from 17.5 [s] to 19.5 [s]. Generated torque for upward movement assistance is in white area, for gravity compensation is in gray area, and for weight bearing assistance is in dark gray area.

The assistance is expected to present effectual movement and sensory stimulation, those are considered to augment brain plasticity and enhance motor function. Several studies verified that training with that information presented from a robot enhanced motor function of a subject [9-12]. In addition, it was reported that voluntary movement promotes brain plasticity [13]. Therefore, we expect that he could acquire a wider range of activities than using wheelchair. Furthermore, by simply repeating using it, the patients' moving ability that is commonly considered being difficult to be enhanced, will be effectively improved.

Though we performed the experiment with a healthy male subject, clinical trials should be performed for application of moving assistance for CP patients. Because it was expected that he adjusted a movement involuntary. He could not completely mimic the movement of a CP patient. And, for assisting daily movement, stair descent assistance should be developed. When HAL could assist daily movement of CP, they will be able to move to anywhere.

VII. Conclusion

In this study, we proposed an automatic control method for stair ascent assistance, and verified the effectiveness of the proposed method. To determine phase transition in stair ascent, we proposed a phase determination method based on height of a landing area, CoGRF of lateral plane and CoGRF of sagittal plane. Our proposed automatic control method assists the motion of each phase. Experimental results showed the method was applicable for assisting walking and stair ascent. In the experiments, the method could determine the phase and generated torque for appropriate movement assistance of each phase during stair ascent. The phase determination could also determine the height of a landing area and switch the control into walking assistance seamlessly. This movement assistance method would help to acquire the range of activity of CP patients.

References

[1] KRÄGELOH-MANN I., CANS C., "Cerebral palsy update", *Brain & development*, vol. 31, no. 7, 2009, pp.537–544.

[2] C. Van den BROECK, J. DECAT, G. MOLENAERS, I. FRANKI, E. HIMPENS, D. SEVERIJNS, K. DESLOOVERE, "The effect of individually defined physiotherapy in children with cerebral palsy (CP)", *Eur. J. Paed. Neurol.*, vol. 30, 2010, pp.1–7.

[3] H. Kawamoto,Y. Sankai, "Power Assist System HAL-3 for Gait Disorder Person", in *Proc. of the 2002 Int. Conf. on Computers Helping People with Special Needs (ICCHP 2002)*, 2002, pp.196-203

[4] T. Hayashi, H. Kawamoto,Y. Sankai, "Control Method of RobotSuitHAL working as Opeartor's Muscleusing Biological and Dynamical Information", in *Proc. of IEEE/RSJ Int. Conf. on Intelligent Robots and Systems*, 2005, pp.3455-3460

[5] T. Taketomi, Y. Sankai, "Walking Assistance for Cerebral Palsy with Robot Suit HAL", *Trans Jpn Soc Med Biol Eng*, vol. 50, no. 1, 2012, pp. 105-11. (In Japanese with English abstract)

[6] A. Protopapadaki, WI. Drechsler, MC. Cramp, FJ. Coutts and OM. Scott, "Hip, knee, ankle kinematics and kinetics during stair ascent and descent in healthy young individuals", *Clin Biomech (Bristol, Avon)*, vol. 22, 2007, pp.203–210

[7] L Mouchnino, ML Mille, M Cincera, A Bardot, A Delarque, A Pedotti and J Massion, "Postural reorganization of weight-shifting in below-knee amputees during leg raising", *Ex- perimental Brain Research*, vol. 121, 1998, pp. 205-214

[8] Tsuchiya K, Imada H, Okawa T, "Activities of daily living", Ishiyaku Publishers, 1992 (In Japanese)

[9] A. Meyer-Heim, I. Borggraefe, C. Ammann-Reiffer, S. Berweck et al., "Feasibility of robotic-assisted locomotor training in children with central gait impairment", *Dev Med Child Neurol*, vol. 49, 2007, pp. 900–906

[10] I. Borggrafe, A. Meyer-Heim, A. Kumar, J. Simon Schafer, S. Berweck, F. Heinen, "Improved gait parameters after robotic- assisted locomotor treadmill therapy in 6-year old child with cerebral palsy", *Mov. Disor.*, vol.23, no. 2, 2008, pp.280– 283

[11] Golomb, M., et al., "In-home virtual reality videogame telerehabilitation in adolescents with hemiplegic cerebral palsy", *Arch Phys Med Rehabil*, vol. 91, 2010, pp. 1-8.e1.

[12] H.I. Krebs, B. Ladenheim, C. Hippolyte, L. Monterroso, J. Mast, "Robot-assisted task-specific training in cerebral palsy", *Developmental Medicine and Child Neurology*, vol. 51, 2009, pp.140-145

[13] F. Gómez-Pinilla, Z. Ying, R. R. Roy, R. Molteni, and V. R. Edgerton, "Voluntary exercise induces a BDNF-mediated mechanism that promotes neuroplasticity", *Journal of Neurophysiology*, vol. 88, 2002, pp.2187-2195

Visual Feedback System Showing Loads on Handrails for Gait Training

Ryotaro Sabe, Tomohiro Hayashi, Yoshiyuki Sankai

Abstract—**Patients with walking difficulties need support devices such as a walker or a cane. However, the support devices sometimes restrict their activities of daily living (ADL). In order to improve the patients' ADL, it is desired that they use the support device that does not restrict their activities as much as possible. The patients need gait training to reduce the dependence on the support device and to switch to a device with fewer restrictions. The purpose of this study is to develop a new visual feedback system that helps the patient receiving gait training to recognize their dependence on the support device. The developed system measures the load that the trainees applied on the handrails, and shows this load graphically by using a display monitor. The walking experiment was carried out with able-bodied subjects in order to ensure that the developed system can give the load feedback to the subjects and they could control the loads on handrails. The experiment was performed in the two cases in which the load information was shown to the subjects, and the load information was not shown to them. During the experiment, the subjects were instructed to adjust the load in accordance with the reference load indicated by the graphical user interface of the developed system. As a result, the subjects could adjust the load to the reference load more appropriately when the load information was given to them. The result, therefore, suggests that the developed system is able to help trainees to be aware of and control the load supported by their arms.**

I. Introduction

Walking is an important part of the activities of daily living (ADL). The patients with walking difficulty need support devices such as walkers or canes to maintain their posture and support their body weight instead of their impaired lower limb. With the help of the support device, the patients can improve their ADL. However, the support device sometimes also restricts their common daily activities. In order to improve the patients' ADL effectively, it is desired that they use the support device that does not restrict their activities as much as possible. The patients need gait training to reduce the dependence on the support device and to switch to a device with fewer restrictions. If the patients can reduce the loads applied on the handrails of support devices from their upper limbs, the dependence on support devices can be reduced. Therefore, it is important for the patients to practice walking in an effort to reduce the loads on the handrails, and switch support devices from such as walkers to canes as shown in Fig. 1.

For the gait training, the trainees need to know whether their body movement is appropriate or not. Commonly, trainers such as a physical therapist (PT) observe the trainee's movement and teach them to walk appropriately. Some information on the body movement, however, is difficult to assess correctly by the observation. Moreover, such information is also difficult to show quantitatively to the trainees verbally. To solve these problems, there are a lot of systems that give a feedback to the trainees [1]-[8]. However, to the best of our knowledge, there is no visual feedback system that can measure the loads on handrails and show them to the trainees objectively in the actual training scene. If such kind of system is developed, it would help patients to reduce the degree of dependence effectively and help them to switch the support devices to that with fewer restrictions in daily living.

The purpose of this study is to develop a feedback system that can indicate the loads on handrails applied by the trainees visually. In addition, the developed feedback system is assessed in a walking experiment with able-bodied subjects to ensure whether they can recognize and control the loads by using the system.

II. Development of a Feedback System

A. System Configuration

Figure 2 shows an overview of the system. The developed feedback system consists of the measurement unit and the display unit. The system has been designed to be attached to a commercially available walker. Two measurement units are respectively attached to the right and left handrails of the walker for measuring the loads on handrails. The display unit is mounted at the center of the walker for showing the loads using a graphical user interface (GUI).

The details of the both units are described in the following subsections.

Manuscript received October 1, 2012.

Part of this work was supported by the "Funding Program for World-Leading innovation R&D on Science and Technology (FIRST Program)," initiated by the Council for Science and Technology Policy (CSTP).

R. Sabe and Y. Sankai are with Cybernics Laboratory, Systems and Information Engineering, University of Tsukuba, Ibaraki 305-8573,Japan (e-mail:sabe@golem.kz.tsukuba.ac.jp,hayashi@golem.kz.tsukuba.ac.jp, sankai@golem.kz.tsukuba.ac.jp)

T. Hayashi is with Tsukuba R&D Center, CYBERDYNE Inc. D25-1, Gakuen Minami, Tsukuba, Ibaraki, 305-0818, Japan (e-mail : hayashi@golem.kz.tsukuba.ac.jp)

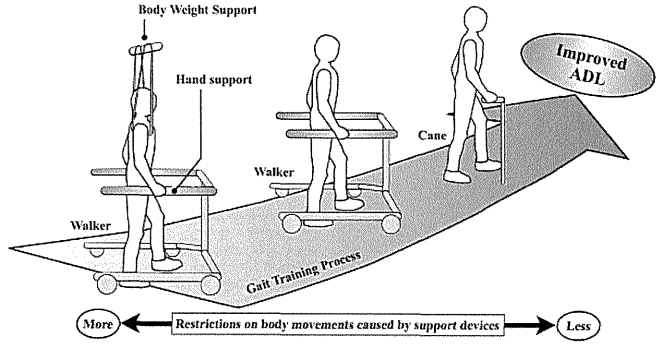

Fig. 1: Gait training process for improving the patients' ADL from the standpoint of the restrictions on body movements caused by support devices.

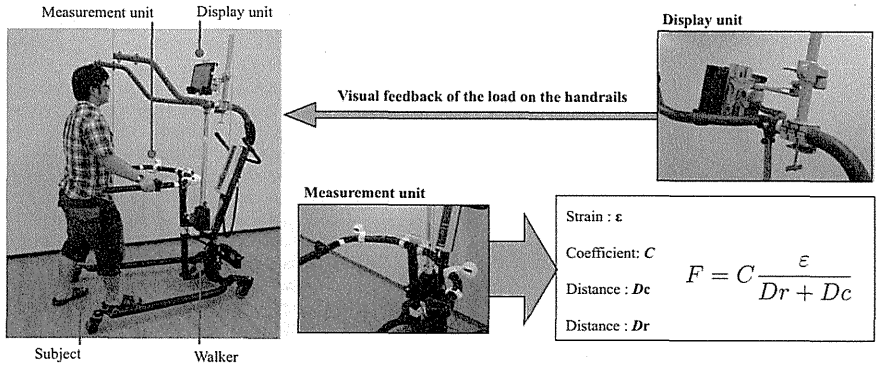

Fig. 2: The developed system for giving the feedback of the loads on handrails to the trainee during gait training. The trainee can know the loads information by looking at the display unit.

B. Measurement unit

The handrail of the walker can be considered as a cantilever beam. On the assumption that the load from the patient is exerted on a point on the handrail, the load on the cantilever beam is shown as

$$F = C\frac{\varepsilon}{D} \qquad (1)$$

where F is the load on the handrail; C is strain coefficient; ε is the strain of the cantilever beam; D is the distance from the load to the point where the strain is measured.

If ε and C are obtained, F can be calculated. In this study, strain gauges and distance sensors were used to obtain them. Figure 3 shows a schematic of the measurement unit. We adopted the two-active gauge method for strain measurement in order to minimize temperature drift. Two strain gauges were attached to the top and bottom surfaces of each the right and left handrail. The developed measurement unit can measure the load caused by a weight suspended from the handrail with an accuracy of ± 5 N.

In order to obtain the distance D, the center of the load on the handrail need to be detected. In this study, we assumed that the center of the load is located at the center of the hand grasping the handrail. Dc in Fig. 3 is the distance from the anterior end of the grasping hand to the center of the load. In order to detect the anterior end of the hand, a distance sensor using infrared light was attached at each head of the handrail. To detect the grasping hand clearly, the reflection module was put just ahead of the hand as shown in Fig. 3. The distance measured by the distance sensor is indicated as Dr in Fig. 3.

The measured strain is amplified and filtered by an analog

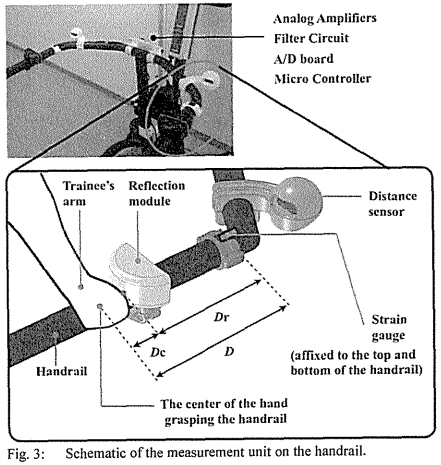

Fig. 3: Schematic of the measurement unit on the handrail.

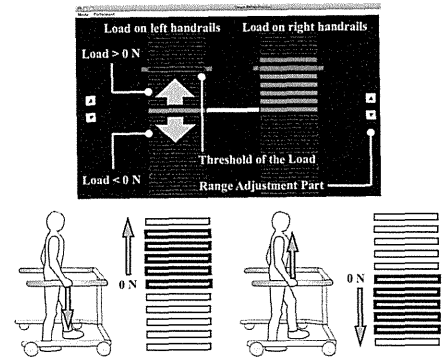

Fig. 4: Graphical User Interface for showing the loads to the trainee while walking. The threshold of the loads and the range for showing loads can be adjusted by using this GUI. The value of the load becomes plus and bar graph extends up when the trainee pushes down the handrails, and the load becomes minus and bar graph extends down when the trainee pulls up the handrails.

preprocessing circuit and converted into digital signals with 100 Hz sampling frequency. The processed signals are transmitted to the display unit via wired Ethernet using the user datagram protocol.

C. *Display unit*

A tablet PC is used as the display unit. It receives the load signals from the right and left measurement units and shows them on its display.

The tablet PC was mounted on the walker by using a monitor arm. The monitor arm is designed to be able to adjust the height and angle of the display of the tablet PC in accordance with each trainee's height.

Fig. 4 shows the GUI screen for showing the load information on the tablet PC. The green bars displayed at the right and left sides on the screen indicate the loads on the right and left handrails respectively. The displayed loads are updated in real time. One step of the bar corresponds to 10N. The threshold value can be chosen for the right and left handrails and inputted into the GUI by the trainer. When the load exceeds the threshold value, the color of the bar graph is changed to red as shown in Fig. 4. By using the different colors, the display unit helps trainees to recognize whether the load exceeds the threshold or not. The range of the load can also be adjusted on the GUI.

In order to reduce influence of noise, the measured load signals are smoothed through a moving average (MA) filter. The window size of the MA filter is set to 100 ms. The smoothed load signals are shown on the display to trainees during training.

III. EXPERIMENTS

A. *Outline*

The experiment with five able-bodied subjects was carried out in order to ensure whether the subjects are able to control the loads on handrails by using the developed feedback system. The subjects were instructed to adjust the loads in accordance with the reference load indicated by the GUI during the experiment. Error rates between the reference load and the measured load were calculated to evaluate the accuracy of the adjustment of the loads on handrails.

To evaluate the feedback system, the experiment consists of the following two trials: a) in which both the loads on handrails and reference loads were shown to the subjects and b) in which only the reference load was shown to the subjects.

B. *Reference Load and Evaluation of Error Rates*

The reference load was given to the subjects as follows.

$$\begin{aligned} W_d(t) &= 50u(t-3) \qquad 3 \le t \le 8 \\ W_d(t) &= -50u(t-13) \qquad 13 \le t \le 18 \end{aligned} \tag{2}$$

where $Wd(t)$ is the reference load; $u(t)$ is a step input; t is elapse time. Here, the time interval $3 \leqq t \leqq 8$ is described as the plus interval, and the time interval $13 \leqq t \leqq 18$ is described as the minus interval. In order to evaluate the developed feedback system in both cases in which subjects adjust the loads by pushing handrails and by pulling handrails, the reference load was set to +50 N and -50 N.

The error rate was evaluated by root means square error (*RMSE*) as

$$RMSE = \sqrt{\frac{1}{T}\sum_{t=1}^{T}\left[W(t) - W_d(t)\right]^2} \tag{3}$$

where $W(t)$ is the loads on handrails; T is the total time spent on showing each reference load. The reduced *RMSE* means that subjects can adjust the loads appropriately in accordance with the reference load.

C. *Protocol*

The walking experiment was carried out with 5 able-bodied subjects in their 20s from AS1 to AS5. The range for showing loads was preliminarily selected from -100 N to 100 N. At first, the subjects were instructed to fix the reflection modules on handrails and positioned the tablet PC according to their height. After finishing this procedure, subjects were instructed by the GUI to start walking and to adjust the loads to the reference load indicated by the GUI. Preliminarily, they were instructed not to be conscious of the loads at the block time when $0 \leqq t \leqq 3$, $8 \leqq t \leqq 13$ and $18 \leqq t \leqq 21$. They were also instructed to walk in a straight line at comfortable speed. The trial b) was carried out 10 times for each subject, and after that, the trial a) was also carried out 10 times for each subject. In order to exclude the effect of practice to the system in the trial b), the result of the loads on handrails was not given to the subjects during the walking experiment. The same reference load was used during the 20 times walking experiment in order to remove effects upon the RMSE caused by the difference of the reference load.

IV. RESULTS

Figure 5 shows the representative result of the walking experiment. From the result, we verified that variance of the load data was reduced by giving the load feedback to AS1 at the plus interval. We also verified that the variance was reduced with the developed system at minus interval. The result of RMSE are shown in Table 1 and Fig. 6. From the results, we verified that the average of the *RMSE* was 50 N at plus interval, and 23 N at minus interval in the trial b). We also verified that the average of the *RMSE* was 17 N at plus interval, and 19 N at the minus interval in the trial a). From this we verified that the *RMSE* was reduced when the load information was shown to the subjects by using the developed feedback system during the walking experiment.

A statistical test was performed to verify whether there is a significant difference between the cases in which the feedback was applied to the subjects and in which the feedback was not applied to them. Since the samples are paired, the dependent t-test for paired samples is used as a statistical test. A significance level of the t-test was set to 5%. As a result, the value of t was 5.31 at plus interval and 4.37 at minus interval. Because the value of t is 3.25 when the significance level of the t-test is set to 1 %, we verified that there was a significant difference in the *RMSE* of the load data both at the plus interval and the minus interval.

V. DISCUSSION

The patients with walking difficulties need support devices in their daily lives because they have difficulty of assisting their own body weight. Hence practicing to reduce the loads on handrails during gait training is beneficial for reducing the dependence on support devices and improving their ADL.

In this study, we developed the new feedback system for gait training. The developed system measures the loads on the handrails of the walker and show that load information to trainees by using the tablet PC.

As the result of the walking experiment with five able-bodied subjects, we verified that both the variance and the RMSE of the load data were reduced in the trial a). By applying the dependent t-test for paired samples, we also verified that the average of RMSE was significantly minor when the load information was shown to the subjects. These results clearly indicate the advantage of the developed feedback system for the trainees to control the loads on handrails appropriately during gait training.

In the walking experiment, considering the both cases in which the trainees pull up handrails and the trainees push down handrails in order to support their own body, we chose reference load -50N and 50N. From results, the variance at the minus interval was less than that at the plus interval in the trial b). Additionally, the RMSE produces the same results as the variance' result. These results mean that subjects could adjust the load more appropriately when -50N was indicated as the reference load by the system. The reason is considered to be that people are used to hold something with their hands while walking, but they are unaccustomed to push something by their hands at a certain amount of force while walking in daily living.

Confining the reference load to 50N and -50N in the walking experiment remains a matter of debate, because the pressure feeling differs in subjects. Thus, about the walking experiment, we did not quantitatively investigate the links between the reference load and the RMSE. However, with respect to the feedback system, we confirmed that the system could show the load information to the subjects and they could control the load more appropriately with the developed system.

In this study, the efficacy of the developed feedback system was verified by the walking experiment with able-bodied subjects. In future research, we plan to evaluate the efficacy of the load feedback by carrying out the experiment with the patients who have walking difficulties. It is important for patients to reduce the load in accordance with the reference load during gait training in an effort to reduce the dependence on support devices and switch support devices to the ones with fewer restrictions. Therefore, adjusting the reference load is believed to be linked to the degree of difficulty of gait training. We plan to investigate the way to adjust the value of reference load to the patients' grade of severity in future research.

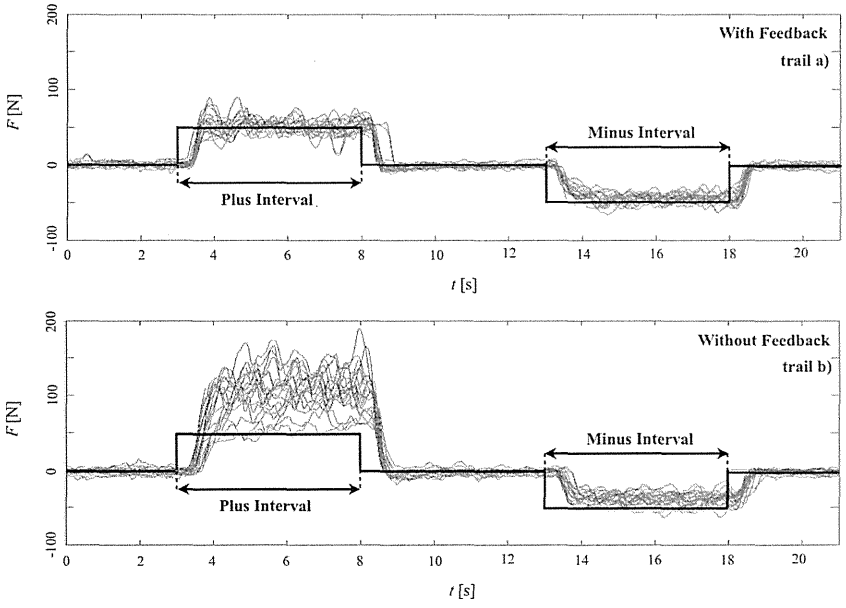

Fig. 5: Result of the walking experiment for AS1 as a representative result. The blue lines show the left load, and the red lines show the right load. The black line indicates the reference load that was set to 50 N at the plus interval and -50 N at the minus interval during the walking experiment. The load data was continuously stored and the error rate was evaluated by RMSE. The RMSE at the plus interval was calculated between t=3 and t=8, and the RMSE at the minus interval was calculated between t=13 and t=18.

Table 1: Result of the RMSE of the loads at the plus interval and the minus interval

Plus Interval

AS ID	Left / Right	RMSE [N] without Feedback	RMSE [N] with Feedback
1		56	17
		55	18
2		43	16
		39	17
3		53	19
		47	17
4		26	17
		25	20
5		87	16
		66	18
Average		50	17
Standard deviation		17.7	1.2

Minus Interval

AS ID	Left / Right	RMSE [N] without Feedback	RMSE [N] with Feedback
1		21	17
		21	18
2		25	22
		23	21
3		26	17
		20	18
4		26	21
		22	19
5		22	21
		22	21
Average		23	19
Standard deviation		2.2	1.7

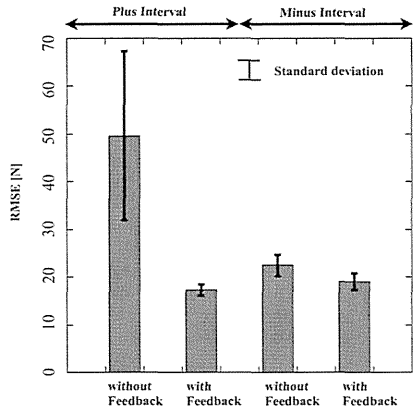

Fig. 6: Result of the RMSE during walking experiment. The bar graphs indicate the average of the RMSE in each case.

VI. Conclusion

In this research, we developed a new feedback system for showing how much load a trainee is applying on handrails during gait training. The developed system was ensured in the walking experiment. The system effectively gives feedback of the load information to the able-bodied subjects and assists them to adjust the load appropriately in accordance with the reference load indicated by the system. This feedback system would help the patients with walking difficulties to improve their gait and improve their ADL.

References

[1] Y. Baram, R. Lenger, "Gait improvement in patießnts with cerebral palsy by visual and auditory feedback," *Virtual Rehabilitation International Conference*, pp.146-149, 2009.

[2] E. Isakov, "Gait rehabilitation: a new biofeedback device for monitoring and enhancing weight-bearing over the affected lower limb," *European Journal of Physical and Rehabilitation Medicine*, Vol. 43, No. 1,pp. 21-26, 2006.

[3] B. Joonbum, K,, Kyouguchi, K., B., Nancy, T., Masayoshi, "A Mobile Gait Monitoring System for Abnormal Gait and Rehabilitation : A Pilot Study for Parkinson Disease Patients." *Journal of Biomechanical Engineering*, Vol. 133, No. 4, pp. 1-11, 2011

[4] J.M. Stacy, A.P. Joseph, "SHOE-INTEGRATED SENSOR SYSTEM FOR WIRELESS GAIT ANALYSIS AND REAL-TIME FEEDBACK", *Biomedical Engineering Society*, Vol. 3, pp. 2468-2469, 2002

[5] A. Ledebt, J. Becher, J. Kapper, R.M. Rozendaalr, R. Bakker, I.C. Leenders, G.J. Savelsbergh, "Balance training with visual feedback in children with hemiplegic cerebral palsy: effect on stance and gait", *Motor Control*, Vol. 9, No. 4, pp. 459-468, 2005

[6] D. Erbil, D. Nigar, A. Duygu, "Effects of biofeedback treatment on gait in children with cerebral palsy", *Disability and rehabilitation*, Vol. 26, No. 2, pp. 116-120, 2004

[7] S. Abhishek, B.T. Arun, G. Anupam, K. Senthil, M. Thyloth, "Post-stroke balance training: Role of force platform with visual feedback technique", *Journal of the Nwurological Science*, Vol. 287, No. 1-2, pp. 89-93, 2009

[8] E. Aiello, D.H. Gates, B.L. Patritti, K.D. Cairns, M. Meister, E.A. Clancy, and P. Bonato,"Visual EMG Biofeedback to Improve Ankle Function in Hemiparetic Gait", *Engineering in Medicine and Biology Society*, pp. 7703-7706, 2005

Wearable Parallel Processing Based High-Resolution High-Speed Electroencephalogram Monitoring Integrated System

Alexsandr I. Ianov, Hiroaki Kawamoto and Yoshiyuki Sankai

Abstract — **Daily use of electroencephalogram (EEG) could increase the effectiveness for medical applications. However, current brain monitoring technologies lack one or more characteristics necessary for daily use, such as portability, responsiveness or versatility. In this study we developed a portable prototype for high resolution real-time EEG monitoring fully integrated system. The prototype is composed of 112 custom made hybrid capacitive-resistive electrodes and up to 7 reference electrodes. The electrodes are connected together by using a flexible, elastic grid which is attached to an adjustable, link based mechanical headgear. Real time processing was performed using a mobile Compute Unified Device Architecture (CUDA) platform for massive parallel processing of the data. Experiments to test the capabilities of the prototype were performed. The first experiment consisted of monitoring the frontal lobe when applying visual stimulus using a lamp. When the lamp was turned on weak alpha waves were detected, while when the lamp was turned off alpha waves were detected. The second experiment consisted of monitoring the entire motor cortex while moving the right hand. At rest, strong mu-rhythm signals were detected over the entire scalp above the motor cortex whereas when moving the right hand mu-rhythm signals above the left motor cortex area were weakened. Both experiment results matched known brain activity phenomena demonstrating basic monitoring capabilities of the prototype. Furthermore we showed that our system has high portability, usability and capable of high responsiveness on high resolution conditions. The concepts introduced in this paper can not only improve EEG monitoring technologies but also contribute to other areas of wearable computing.**

I. Introduction

BRAIN activity monitoring technologies are fundamental tools in the treatment of neurological disorders, rehabilitation techniques, assistive device interfacing methods[1]-[3] and are becomes increasingly important in social and entertainment aspects of wearable computing. Depending on the patient or situation, constant monitoring during daily life is desirable or required. Electroencephalography (EEG) monitoring has been traditionally suggested for daily brain activity monitoring as compared to Magnetic Resonance Imaging (MRI) or Magnetoencephalography (MEG) it is a much cheaper, smaller and versatile solution.

Manuscript received September 18, 2012. Part of this work was supported by the "Funding Program for World-Leading Innovative R&D on Science and Technology (FIRST Program)," which was initiated by the Council for Science and Technology Policy (CSTP).

All the authors are with Cybernics Laboratory, System and Information Engineering, University of Tsukuba, Ibaraki 305-8573, Japan (e-mail: ianov@golem.kz.tsukuba.ac.jp; kawamoto@golem.tsukuba.ac.jp; sankai@golem.tsukuba.ac.jp).

Several EEG technologies are available commercially[4]. Systems such as the BCI2000[5] and the G.Tec (Guger Technologies, Austria) are widely used in medical and academic facilities. Such systems are capable of high spatial and temporal resolution. However these products rely on passive resistive electrodes requiring the user to perform skin preparation and lose signal quality with time[6]. Moreover such devices are used as nonwearable computer peripherals, as the headgear and electrodes are connected through a series of cables to a standalone Analog-Digital Converters (ADC) unit which is connected to a host personal computer (PC). This design limits the motion freedom of the user and application scope of the system due to the low portability and usability.

By contrast, systems such as the Epoc headset (Emotiv Systems, Australia) or the Mindwave headset (Neurosky Inc., USA) have been developed targeting entertainment applications. These systems are characterized by having high portability and wearability. However, due to the fixed mechanical design they lack the versatility required for several medical and academic applications. Moreover, the limited onboard processing power limits maximum number of channels a headset can have and an external PC is still required for several applications. Furthermore the lag originated from the wireless connection between the PC and the headset is an issue when real-time processing is required.

From an end-user point of view, brain activity monitoring requires a device with high usability and portability that minimizes the impact on daily life of the end-user. From a professional point of view, a device should provide high spatial and temporal resolution for high responsiveness and signal reliability, it should be strong against noise sources and it also should be flexible enough to provide the opportunity for a wide range of applications over the same platform. A common device that can be used by both professionals and end-users would streamline application development as well as increase data consistence. However such device would also require high usability, portability from the end-user requirements as well as the high versatility and reliability from the professional requirements. In previous researches the authors have developed a hybrid capacitive-resistive electrode for bioelectrical signal capable of signal quality comparable with commercial electrodes achieving high reliability while also achieving high usability as no skin preparation is required and the signal does not degrade with time[7][8]. Furthermore, while mobile Central Processing Units (CPUs) are not fast enough to perform data collection and frequency analysis simultaneously and in real time of a large number of sensors at high sampling frequencies, the parallel nature of EEG monitoring is compatible with the concepts of parallel processing using Graphic Processing Units(GPUs). Other researchers have already demonstrated the signal processing capabilities and significant performance advantages of GPUs using Compute Unified Device Architecture (CUDA)[9][10]. By integrating our hybrid electrodes with a mobile, onboard GPU based data processing system using a modular design, a novel wearable all in one EEG monitoring device that provides simultaneously high usability, portability, versatility and reliability can be achieved.

In this study we develop a novel integrated EEG monitoring system combining capacitive bioelectrical measurement and parallel computing technologies. A portable high-resolution EEG monitoring headgear composed of up to 112 sensing electrodes and up to 7 reference custom hybrid capacitive-resistive electrodes was developed. In order to record and analyze the massive amount of data from the headgear, a CUDA based wearable processing system was developed providing real-time signal analysis for each sample at 1 kHz sampling rates.

II. Materials and Methods

A. Hardware Development

In this study hybrid resistive-capacitive electrodes that we previously developed were used as EEG sensors[7][8]. EEG recordings are performed throughout active resistive contact with when the electrodes are capable of electromechanical contact(resistive mode). However, in the case of poor contact conditions, the electrodes capacitive couple with the scalp in order to perform the readings(capacitive mode). Fig.1 shows the equivalent circuit when the electrodes are in use. This model also includes noise from capacitive sources as

$$V_{IN} = \frac{R_c}{Z_{nc}} V_{nc} + \frac{R_c}{Z_{nsei}} V_{nsei} + \frac{R_c}{Z_{sei}} V_{BES} \quad (1)$$

where V_{bes} is the bioelectrical signal voltage, V_{in} is the electrode input voltage, V_{nsei} is the total noise source voltage at the skin-electrode surface, V_{nc} is the total noise source voltage on the electrode board, Z_{sei} is the skin-electrode interface impedance, R_c is the electrode input impedance, Z_{nsei} is the noise input impedance at the skin-electrode interface, and Z_{nc} is the noise input impedance on the electrode board. This noise can be significant if the electrodes are in capacitive mode. However it can be minimized when the sensor input impedance is optimal, when it is large enough to make the sensor electrode to capacitive EEG signals but low enough to reject capacitive noise signals from the environment. Input impedance is optimized using

$$R_c = \frac{V_{IN}}{V_{BES}} \cdot \frac{d}{\varepsilon_r \varepsilon_0 A 2\pi f} \quad (2)$$

where ε_0 is the dielectric constant in vacuum, ε_r is the relative dielectric constant to the material, A is the electrode lead sensing area nearest to the skin, f is the frequency of the target signal and d is the distance between the skin and the electrode lead.Based on this model and assuming a maximum 1 mm distance between the electrode and the scalp, an electrode measuring 14 mm^2, with total sensing area of 8 mm^2, and input impedance of 1 TΩ was developed. Noise frequency spectrum measurement experiments were performed for both resistive and capacitive modes by placing two electrodes face to face on differential input. The results are shown in Fig. 6, Chapter 3.

119 hybrid electrodes were used to assemble a headset, as shown in Fig. 2 and Fig. 3. The headset is composed of two main elements. The first element is a variable link mechanism designed using statistical head anatomical data provided by the Japanese National Institute of Advanced Industrial Science and Technology (AIST)[11]. The flexibility provided by using an articulated link mechanism allows the headset to fit on wide range of head geometries. The second element is an elastic net which is attached to the link mechanism. The elastic net is responsible for keeping the link mechanism closed when worn due to the elastic force towards the inside to the headset as well as being the docking place for the electrodes.

The electrodes are placed as shown in Fig. 4. This placement method is fully compatible with the International 10-20 Method for EEG electrode placement. The electrodes are divided in 7 groups of 16 measurement channels and 1 reference for a total of 112 channels and 7 references. The option for having using only one reference electrode for all measurement channels is also available. Each electrode group is connected to a differential input capable 16 channel 16 bit ADC module as shown in Fig. 5. All electrodes and modules can be freely added or removed based on the user's need. All modules are connected through USB 3.0 to a dual core Intel Atom Based mother-board with a CUDA capable Nvidia Ion 2 chipset.

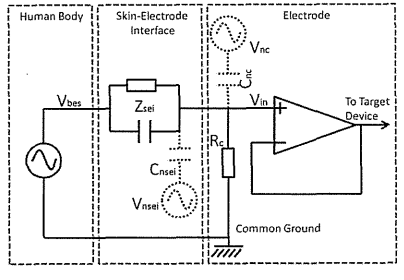

Fig. 1. Electrode equivalent circuit

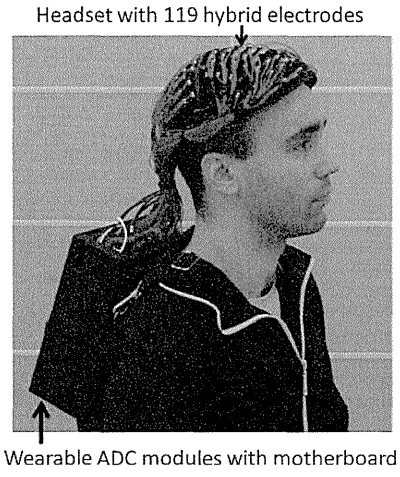

Fig. 2. EEG monitoring integrated system

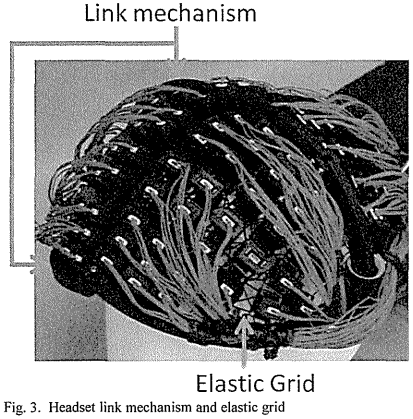

Fig. 3. Headset link mechanism and elastic grid

All the ADC modules, the mother-board and the battery are located in a wearable backpack. The headset weighted 745 g and the backpack weighted 1.80 kg. Data can be stored locally and visualized through an external display or PC.

B. Signal Processing System

EEG signals were recorded as a differential signal between a channel electrode and a reference electrode. Signal is amplified, filtered and sampled at 1 kHz at the 16 bit ADC modules. ADC modules simultaneously send the data to the motherboard CPU which stores the data on the memory. Using a different thread, the CPU sends the signal processing instructions and to the GPU.

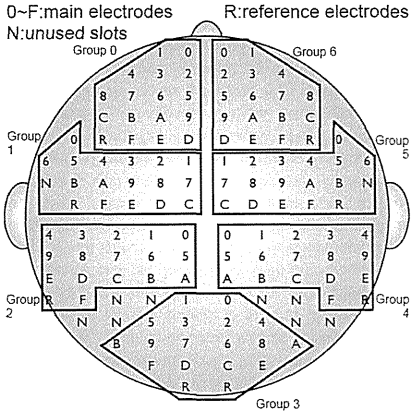

Fig. 4. Electrode placement method

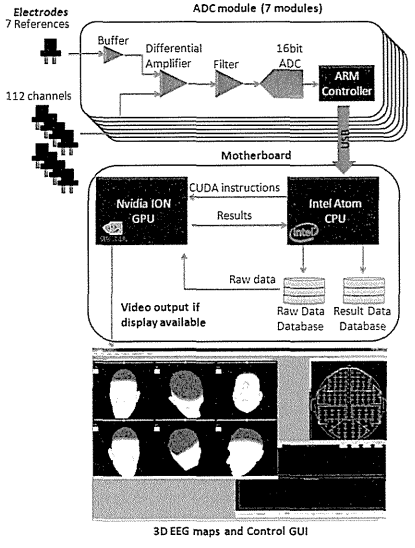

Fig. 5. Hardware elements and data flow diagram

In this preliminary study we demonstrate the capabilities of wearable GPU based processing for EEG monitoring by performing real time Fast Fourier Transforms (FFT) for all channels in real time on the GPU. Ideally, in our approach, we would perform a FFT based on the Cooley-Tukey algorithm for each channel using a separate GPU thread. However, due to the limitations on number of cores available in the used mobile GPU, we used the minimal recommend 32 CUDA threads, each thread performing the FFT from 4 channels. Because our system had only 112 channels, for code simplicity, we created an additional 16 dummy channels group with duplicated data from real channels to bring the total number of channels to 128. Channel data acquisition and result output is performed using the GPU direct memory access features. Each FFT was performed using the latest 1024 data samples for each channel, after each sampling cycle finished. FFT results are mapped on a human head 3D model for showing EEG signal strength at a chosen frequency at any point of the user's head. The 3D map can be visualized alongside the control graphical user interface for system by plugging in an external monitor or remotely accessing the systems.

C. EEG Monitoring Experiments

Two standard experiments monitoring EEG signals from different areas of the scalp were performed for device testing.

The first experiment consists in measuring brain activity changes above the frontal lobe due to visual stimuli. Previous studies have shown that when visual stimulus is weak, such as when the eyes are closed are the subject is in dark places, it's possible to record strong signals in the alpha band (8-13Hz) on the scalp area above the frontal lobe of the human brain[12][13]. In this experiment we perform EEG recordings by placing the participants on a dark room. A lamp was positioned in front of the participant and is used as an external source of light and visual stimuli. The lamp was turned on and off every 15 seconds during the total experiment time of 120 seconds.

The second experiment consists in measuring brain activity changes above the motor cortex that are due to hand and finger motions. When the participants' intention of movement is small, such as when the subject is at rest, it's possible to record strong signal on the 10 Hz u-rhythm frequency range, in the area above the motor cortex of the human brain. On the other hand, when the participant is moving one hand, u-rhythm gets weaker above the motor cortex opposite to the hand[14][15]. In this experiment we perform EEG recordings by placing the participants on a dark and silent room with the eyes closed. The subject stayed motion less for 30 seconds and then moved the right hand on a finger tapping movement, for another 30 seconds. This cycle was repeated 2 times for each experiment for a total experiment time of 120 seconds.

In order to evaluate the impact of the use of the GPU, both experiments were performed with and without using the CUDA features described in Section 2.2. The experiments were performed with 2 participants, each experiment was performed 3 times.

III. Results

A. Hybrid Electrodes

The noise spectrum in the 1-100 Hz band is shown in Fig. 6. The results show that noise is bellow 3 $\mu V/Hz^{1/2}$ for both resistive and capacitive modes. As EEG signals are in the order of 10-100 μV and commonly used signals oscillate in the 10-40 Hz band, the results show that our hybrid electrodes are reliable enough for EEG measurements.

B. EEG Monitoring Experiments

For the first experiment, the developed system was capable to record the data on both participants as expected from the results of previous researches. All electrodes showed strong signals when the light was turned off whereas a weak signal was recorded when the light was on. Fig.7 shows a sample spectrogram with the data collected by electrode 0 on group 0.

For the second experiment, the developed system was also capable to record the data on both participants and the results matching previous researches. For both participants, when the participant is performing the finger tapping motion, the electrodes C, D, E, F located on group 1 (Fig. 4) of the system, above the left motor cortex, recorded alpha band signals weaker than the when the participant was at rest. Fig. 8 shows the sample spectrogram for electrode C in group 1.

When experiments were executed with the CUDA features described in Section 2.2, the system was able to record data from all 112 channels at 1 kHz and perform FFTs for all channels after each sampling without delay or data loss. On the other hand, without using the CUDA features, thus allocating all the stress entirely on the CPU, the system took 400 ms to finish the FFTs for all channels and was unable to keep up with the 1 kHz sampling rate.

IV. Discussion

The experiments have shown that our electrodes were capable of recording both alpha waves and μ-rhythm without the need for skin preparation and that the results from our system are matched known brain activity phenomena. Our noise frequency analysis shows that our hybrid electrodes have a noise level below 3 $\mu V/Hz^{1/2}$, performing at similar levels to commercially available electrodes[8][16]. Both experiments suggest our system provides the high reliability required by professionals and end-users.

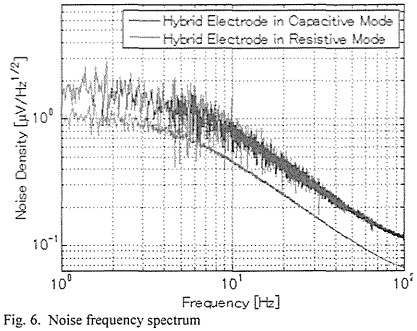

Fig. 6. Noise frequency spectrum

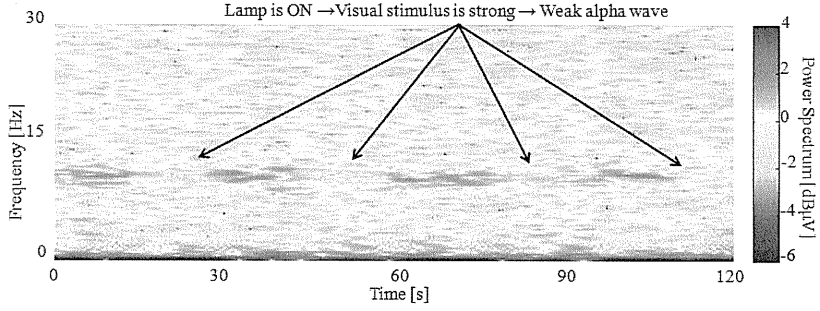

Fig. 7. EEG sample response to visual stimulus

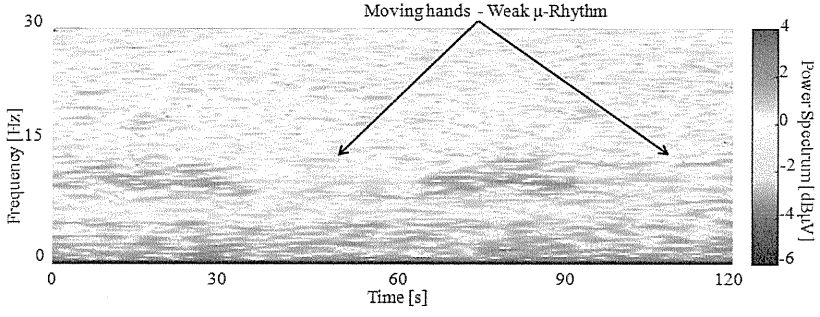

Fig. 8. EEG sample response to motor stimulus

With our hybrid electrodes removed the need of skin preparation, the wearability of the system was further increased by using a novel mechanism the allows the placement of over a hundred EEG electrodes over the users scalp simultaneously, thus reducing the time for wearing our 119 electrode system to up to 5 minutes, similar to the time required for 1-16 electrode systems[4]. Quick and easy electrode placement is fundamental for daily life usage, as it gives the user time to perform other activities while also it does not require specialized staff or training for correctly wearing the system. Furthermore, the lack of conductive gel and the problems associated with it such as signal degradation over time are completely avoided rendering battery capacity the only limiting factor for long continuous monitoring sessions. Using hybrid capacitive-resistive electrodes provided a high usability required by end users while also increasing the reliability of the system without reducing the spatial resolution of the sensor network.

The experiments have shown that our GPU based signal processing algorithm is powerful enough to perform FFTs for each channel after each sampling is finished, at 1 kHz sampling rate. While sampling at 1 kHz is a common practice, performing FFTs for each sampling at this rate is excessive considering the relatively low frequency EEG bioelectrical signals oscillate. However in this study, by showing that our system can perform heavy calculations at very fast rates, we show that our system perform in real time under heavy load by using algorithms optimized for parallel processing. On a realistic application scenario we can reduce the FFT execution and use the GPU processing power for other parallelizable tasks, such as neural networks[17]. Offloading signal processing to the GPU using CUDA not only allowed us to perform frequency analysis at real time but also freed the CPU for writing data to the hard-disk as well as displaying a fully interactive GUI with a 3D map of the EEG signals over the scalp. The high speed data processing allowed us to support a high spatial and temporal resolution which increase the reliability of the signal while leaving the CPU free for user interaction contributing in increasing the usability of the system. Furthermore, using a mobile GPU allowed us to have all these advantages in a wearable package, achieving a system with high portability and removed the need to have an external host PC, creating an all-in-one integrated system.

The data transfer between the electrodes and the GPU equipped mother-board was performed by seven 16-channel modules. This modular design allows users to add or remove at will. Taking advantage of this design professional users can perform experiments and development using high-density sensor networks, whereas when supplying the EEG monitoring system for the end user they can easily reduce hardware and optimize the system for the target application while still maintaining system consistence, thus reducing costs but offering a high application flexibility. In this study our system was a proof-of-concept prototype, thus also containing not optimized off-the-shelf parts, such as the motherboard containing the GPU. With the popularization of GPGPU capable System on Chip devices such as the Tegra 3 (Nvidia Corporation, USA) processor, further miniaturization and increase in power efficiency can be achieved in the near future.

EEG signals are used extensively on sleep disorder diagnosis and treatment, assistive device control and neurorehabilitation[1]-[3]. The effectiveness of some of these applications can be dependent on the frequency at which the patient uses EEG monitoring systems and is able to provide feedback to oneself as well as to the medical staff. While testing our new integrated system on a clinical environment is required, our tests with healthy participants suggest that the techniques in this study are a step forward in to increasing the impact of EEG technologies have in the medical field. Furthermore, the techniques introduced in this study can be extended towards other fields of wearable computing, robotics and medicine.

V. Conclusion

In this study we developed a novel integrated EEG monitoring system combining capacitive bioelectrical measurement and parallel computing technologies. A portable high-resolution EEG monitoring headgear composed of 112 sensing electrodes and 7 reference custom hybrid capacitive-resistive electrodes was developed. In order to record and analyze the massive amount of data from the headgear, a CUDA based wearable processing system was developed providing real-time signal analysis.

In future works we plan to optimize the hardware modular design of our system towards the creation of a EEG monitoring platform that can easily be customized by the users according to their needs as well as testing the device on clinical environments. We also extend the CUDA algorithms beyond real-time frequency analysis into a software platform for rehabilitation training feedback and assistive device interfacing as well as applying its principles to other wearable computing applications.

References

[1] M.L. Fantini, M. Michaud, N. Gosselin, G. Lavigne and J. Montplaisir: "Periodic leg movements in REM sleep behavior disorder and related autonomic and EEG activation", Neurology, Vol. 59, No. 12, 1889-1894 , 2002

[2] J.K. Chapin, K.A. Moxon, R.S. Markowitz, M.A.L. Nicolelis: "Real-time control of a robot arm using simultaneously recorded neurons in the motor cortex", Nature Neuroscience, Vol. 2, pp.664-670, 1999

[3] K.K. Ang, C. Guan, K.S.G. Chua, B.T. Ang, C. Kuah, C. Wang, K.S. Phua, Z.Y. Chin, H. Zhang: "Clinical study of neurorehabilitation in stroke using EEG-based motor imagery brain-computer interface with robotic feedback," 2010 Annual International Conference of the IEEE Engineering in Medicine and Biology Society, pp.5549-5552, 2010

[4] C.T. Lin, L.W. Ko, M.H. Chang, J.R. Duann, J.Y. Chen, T.P. Su, T.P. Jung, "Review of Wireless and Wearable Electroencephalogram Systems and Brain-Computer Interfaces – A Mini-Review." Gerontology, Vol. 56, pp. 112-119, 2010

[5] G. Schalk, D.J. McFarland, T. Hinterberger, N. Birbaumer, J.R. Wolpaw, "BCI2000: a general-purpose brain-computer interface (BCI) system," Biomedical Engineering, IEEE Transactions on , vol.51, no.6, pp.1034-1043, June 2004

[6] J.R. Wolpaw,N. Birbaumer,W.J. Heetderks,D.J. McFarland,P.H. Peckham,G. Schalk, E. Donchin, L.A. Quatrano, C.J. Robinson,T.M. Vaughan,"Brain-computer interface technology: a review of the first international meeting," IEEE Transactions on Rehabilitation Engineering,Vol.8, No.2, pp.164-173, 2000

[7] A. I. Ianov, H. Kawamoto, Y. Sankai, "Development of a Capacitive Coupling Electrode for Bioelectrical Signal Measurements and Assistive Device Use", Proceedings of the 2012 ICME International Conference on Complex Engineering, pp. 593-598, July, 2012

[8] A. I. Ianov, H. Kawamoto, Y. Sankai, "Development of Hybrid Resistive-Capacitive Electrodes for Electroencephalogram and Electrooculogram", IEEJ Transactions of Sensors and Micromachines, Vol. 133, No. 3, 2012(Accepted for publication, in press)

[9] J.A.Wilson, J.C. Williams, " Massively Parallel Signal Processing using the Graphics Processing Unit for Real-Time Brain–Computer Interface Feature Extraction", Front Neuroengineering, Vol. 2, Article 11, 2009

[10] A. Nukada, Y. Ogata, T. Endo, S. Matsuoka, "Bandwidth intensive 3-D FFT kernel for GPUs using CUDA," High Performance Computing, Networking, Storage and Analysis, 2008. SC 2008. International Conference for , pp.1-11, 15-21 Nov. 2008

[11] AIST,"RIO-DB: Available Database", http://riodb.ibase.aist.go.jp/dhbodydb/index.php.ja, March 6th, 2012 [September 14th, 2012]

[12] A. Craig, P. McIsaac, Y. Tran, L. Kirkup, A. Searle, "Alpha wave reactivity following eye closure: a potential method of remote hands free control for the disabled," Technology and Disability, Vol. 10, No. 3, pp. 187-194, January 1999

[13] A. Craig, Y. Tran, P. McIsaac, P. Moses, L. Kirkup, A. Searle. "The effectiveness of activating electrical devices using alpha wave synchronisation contingent with eye closure," Applied Ergonomics, Vol. 31, No. 4, pp. 377-382, August 2000

[14] A. R. Luft, S. McCombe-Waller, J. Whitall, L. W. Forrester, R. Macko, J. D. Sorkin, J. B. Schulz, A. P. Goldberg, D. F. Hanley, "Repetitive Bilateral Arm Training and Motor Cortex Activation in Chronic Stroke", JAMA., Vol. 292(15):1853-1861, 2004

[15] T. Balla, A. Schreibera, B. Feigeb, M. Wagnerc, C. H. Luckinga and R. K. Feig, "The Role of Higher-Order Motor Areas in Voluntary Movement as Revealed by High-Resolution EEG and fMRI," NeuroImage, Vol. 10(6), pp. 682-694, 1999

[16] Y.M. Chi, T.P. Jung, G. Cauwenberghs: "Dry-Contact and Noncontact Biopotential Electrodes: Methodological Review", IEEE Reviews in Biomedical Engineering, Vol.3, pp.106-119 , 2010

[17] H. Jang, A. Park, K. Jung, "Neural Network Implementation Using CUDA and OpenMP," Computing: Techniques and Applications, 2008. DICTA '08.Digital Image, pp.155-161, 1-3 Dec. 2008

生体医工学
50(1)：105-110, 2012

研　究

ロボットスーツHALによる脳性麻痺患者の歩行支援に関する研究

武富　卓三*・山海　嘉之*

Walking Assistance for Cerebral Palsy with Robot Suit HAL

Takumi TAKETOMI,* Yoshiyuki SANKAI*

Abstract The purpose of this study is to propose a method of a walking assistance by using an exoskeletal system "Hybrid Assistive Limb (HAL)" for cerebral palsy (CP) patients who cannot stand up and walk due to the abnormal generation of the bioelectrical signals (BES) in their lower limbs associated with the brain disease, and to verify the effectiveness of the proposed method through a clinical trial. HAL was developed to support the voluntary movement of the wearer based on the BES. The proposed method consists of two algorithms, that is, an assistance of voluntary movement in the swing phase and an assistance of weight bearing in the stance phase. The assistance of the voluntary movement determines the rotational direction of the actuator from the ratio of the abnormal BES by using sigmoid function during the swing phase. On the other hand, the assistance of the weight bearing adjusts automatically the stiffness and viscosity of the joint during the stance phase. In the clinical walking trial with a 3-meter walk using parallel bars, we confirmed that HAL including the proposed method achieved the patient's walking assistance. Especially, the assistance of the voluntary movement in the swing phase produced his leg-swing based on the BES signals. As a result, the walking speed, cadence and stroke width of the patient with HAL during this trial are 1.6 m/min, 11.4 steps/min and 0.14 m, respectively. In conclusion, we have proposed the method of the walking assistance method and thus, confirmed the effectiveness of the proposed method.

Keywords : biomedical signal processing, motor function support, cerebral palsy, robot suit.

1. はじめに

脳性麻痺は，毎年，新生児1000人に3人程度の確率で発生しており，88%の患者が痙直型麻痺を有している[1]．痙直型麻痺患者の中でも対麻痺，四肢麻痺患者は，両下肢にみられる麻痺の影響により移動能力が制限され，補助具を用いた場合においても歩行が困難である場合，車いすでの生活を余儀なくされる．車いすの使用は，環境的要因によって活動範囲が制限されるだけでなく，筋力の低下，関節の拘縮，骨密度の低下といった，様々な身体的悪影響を併発する可能性が高い．このような問題を解決するためには，痙直型麻痺患者の随意的な歩行を実現することが極めて重要である．我々は装着者の身体機能を強化，拡張，補助するための外骨格型ロボットスーツHALを開発している．また，装着者の生体電位信号（BES：Bioelectrical Signal）を用いる随意的制御を提案している[2-4]．BESは，神経・筋活動を反映した信号の一つであることから，関節運動が困難なほど筋力が弱い状況でも計測が可能である．そのため，この制御手法は，筋の発達が未熟な脳性麻痺患者を対象とした随意性を有する動作支援として期待できる．しかしながら，脳性麻痺患者は運動野に受けた損傷によってBESに異常を有することが想定される．したがって，脳性麻痺患者の異常なBESから随意的な操作を判別し，歩行の実現を支援する手法開発の必要性は極めて高い．

本研究ではロボットスーツHALによる脳性麻痺患者の随意的な歩行支援を実現するため，単独での歩行が不可能な脳性麻痺患者1名を対象とした随意的動作支援手法と，HALが自律的に歩行姿勢を管理する制御手法を混在させた歩行支援手法を提案し，実証試験を通じて有効性を確認する．

生体医工学シンポジウム2011発表（2011年9月，長野）
2011年7月29日受付，2011年10月24日改訂，2011年12月7日再改訂
Received July 29, 2011; revised October 24, 2011, December 7, 2011.
* 筑波大学大学院システム情報工学研究科
Graduate School of Systems and Information Engineering, University of Tsukuba

2. 方　　法

2·1 BES計測試験

随意的制御を適用する事前試験として，痙直型麻痺を有する試験協力者が困難としている膝関節の屈伸動作時に発生する膝関節屈筋群・膝関節伸筋群のBESを計測する．なお，本研究は筑波大学の倫理委員会の承認を得た後，試験協力者から書面にて同意を得て実施した．

本試験の協力者は上下肢に痙直を有する14歳男性である．0歳時，脳室内出血を起こしたことにより脳性麻痺を発症し，3歳より自走式車椅子を使用している．移動機能は四つ這いまでであり，訓練として理学療法，作業療法を継続して受けている．また，5歳時に座位の安定を目的としたハムストリングの選択的筋解離術を受療している．

図1に示すように試験協力者はサドル付きの歩行器に乗り，計測側の脚を離地させた状態となる．膝関節屈伸動作は観測者が任意のタイミングで指示し，試験協力者は指示が出されるまで脱力した状態で待機する．動作中に発生するBESは膝関節屈筋群である半腱様筋，大腿二頭筋，伸筋群である大腿直筋，外側広筋の計4カ所に電極を貼り付けて計測する．計測した信号から神経・筋活動の大きさを得るために行う平滑化処理は，これまで開発されてきた生体電位信号処理と同じ手法を用いる[4]．健康状態による傾向の変化を確認するため，Day1とDay2の間には20日間の休憩を設ける．また，同様の計測試験を20代男性の健常者を対象として行い，試験協力者と健常者のBES出力傾向を比較する．

計測試験で得られた信号をセンサ測定範囲の最大値で正規化した結果を**図2**に示す．屈曲動作時において図2(a)に示すように，屈筋群のみから顕著にBESが発生し，健常者と同様な傾向が得られた．しかしながら，伸展動作時では図2(b)に示すように，屈筋群からも顕著にBESが計測され，健常者と異なる傾向が得られた．

2·2 脳性麻痺患者の随意的動作支援手法

本節では，脳性麻痺患者の随意的動作を支援するHALの制御方法について説明する．本研究では，歩行に必要な下肢動作をアシストすることが目的であるので，膝関節と股関節の屈曲・伸展を行うアクチュエータを有する下肢用のロボットスーツHALを用いる．足関節については一般的な歩行訓練と同様に，必要に応じて装具等により固定することとする．

事前試験の結果，試験協力者は伸展動作時において屈筋BESの異常な出力が確認された．したがって，装着者の意図する脚動作をHALによって支援するためには，異常な屈筋BESから適切な支援トルクを生成する手法が必要である．

そこで本研究では，屈曲ならびに伸展時において屈筋BESが全体のBES出力に占める割合を用いて関節の回転方向を判別し，BES出力の強度に応じた支援トルクの生成手法を提案する．

屈筋BESが占める割合xは，以下のように算出される．

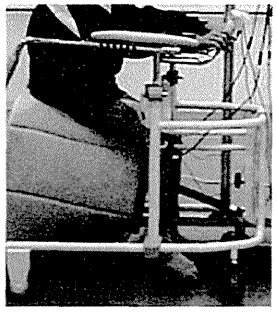

図1 試験環境
Fig. 1 Experimental environment.

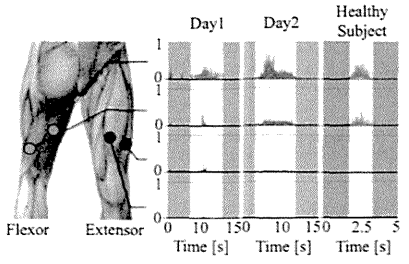

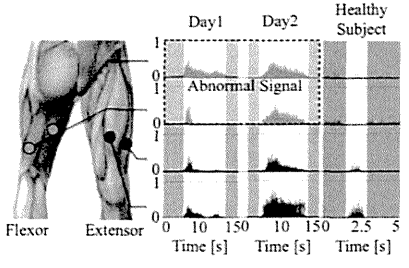

図2 BES計測結果
(a) 屈曲動作時における正規化されたBES
(b) 伸展動作時における正規化されたBES
Fig. 2 Result of BES measurement.
(a) Normalized BES during knee flexion
(b) Normalized BES during knee extension

$$x=\frac{e_{fl}}{e_{ex}+e_{fl}} \quad (1)$$

ただし，e_{fl}，e_{ex} はそれぞれ屈筋と伸筋の BES である．

式(1)で算出された値から支援トルクの回転方向を決定する判別式は，式(2)に示すシグモイド関数を用いる．

$$\sigma_a(x)=\frac{1}{1+e^{-ax+b}} \quad (2)$$

ただし，a，b は任意の定数値である．

提案する随意的動作支援手法のトルク生成式を式(3)に示す．

$$\tau_{est}=\begin{cases}(2\sigma_a(x)-1)\cdot K_{ex}\cdot e_{ex}(\sigma_a(x)<0.5)\\(2\sigma_a(x)-1)\cdot K_{fl}\cdot e_{fl}(\sigma_a(x)<0.5)\end{cases} \quad (3)$$

ただし，τ_{est} Nm は随意的動作支援トルク，K_{ex} は伸展のアシストゲイン，K_{fl} は屈曲のアシストゲイン，x は屈筋 BES が占める割合である．

シグモイド関数は単調増加関数であることから，提案手法を用いることにより，回転方向反転時にトルク出力値を連続的に変化させることが可能である．さらに装着者の意思に応じて変化する BES 出力の強度をトルクの出力値に反映させることで直感的な随意的動作支援を実現できる．

2·3　歩行支援手法

歩行の周期は足部が離床中の期間である遊脚期と，足部が着床中の期間である支持脚期の2種類に大きく分類される[5]．本研究では脳性麻痺患者の歩行支援として遊脚期と支持脚期を各々の動作に適した制御手法で支援し，矢状面における床反力中心に基づいて歩行状態を判別することで各々の制御を連続的に移行する手法を提案する．

2·3·1　遊脚期支援制御　遊脚期は脚を持ち上げ，前方へ振り出す期間である．遊脚における各動作の開始は随意的に行われることから，遊脚動作に対し，本研究が提案する随意的動作支援手法を用いた支援が有効である．したがって，遊脚期動作の支援として随意的動作支援手法と粘性補償制御，重力補償制御を組み合わせた遊脚期支援制御を行う．

粘性摩擦補償トルク τ_{Dcomp} Nm は，アクチュエータの粘性を D_{act} とすると式(4)で与えられる．

$$\tau_{Dcomp}=D_{act}\dot{\theta}_h \quad (4)$$

ただし，θ_h rad/sec は関節角速度である．

重力補償制御は，**図3**(a)，図3(b)に示すようにHALを2自由度のリンク構造としてモデル化することで，重力によってHALの各関節に発生するモーメントを算出し，そのモーメントに拮抗するトルクを出力する．

$$\begin{aligned}\tau_{g\_hcomp}=&\frac{1}{2}\cdot m_{thigh}\cdot g\cdot l_{thigh}\cdot\sin(\theta_{abs}-\theta_h)\\&+m_{shank}\cdot g\cdot\{l_{thigh}\cdot\sin(\theta_{abs}-\theta_h)\\&+\frac{1}{2}\cdot l_{shank}\cdot\sin(\theta_{abs}-\theta_h+\theta_k)\}\end{aligned} \quad (5)$$

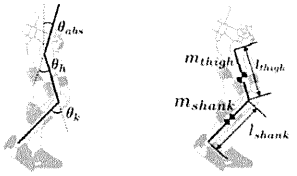

図3　下肢の2リンクモデル
(a) 関節角度
(b) 質点位置

Fig. 3　2 Degree of freedom link model of leg.
(a) Joint angle
(b) Mass Position

$$\tau_{g\_hcomp}=\frac{1}{2}m_{shank}\cdot g\cdot l_{thigh}\cdot\sin(\theta_{abs}-\theta_h+\theta_k)$$

ただし，τ_{g_hcomp} Nm は股関節の重力補償トルク，τ_{g_kcomp} Nm は膝関節の重力補償トルク，θ_{abs} rad は体幹の絶対角度，θ_h rad は股関節の関節角度，θ_k rad は膝関節の関節角度，m_{thigh} kg は大腿の重量，l_{thigh} m は大腿長，m_{shank} kg は下腿の重量，l_{shank} m は下腿長，g は重力加速度である．最終的な遊脚期支援制御のトルク τ_{sw} Nm を式(6)に示す．

$$\tau_{gcomp}=\begin{bmatrix}\tau_{g\_hcomp}\\\tau_{g\_kcomp}\end{bmatrix}$$

$$\tau_{sw}=\tau_{est}+\tau_{Dcomp}+\tau_{gcomp} \quad (6)$$

2·3·2　支持脚期支援制御　支持脚期は体重を支持しながら体幹を推進する期間である．健常者は支持脚中，体幹を直立させ，膝関節を伸展位に維持することで体重支持を行っている．しかしながら，試験協力者は下肢の運動機能が低下しているため，健常者と同様な姿勢の維持が困難である．したがって，HALが自律的に動作を生成する自律制御を用いて体重支持に適した姿勢を管理し，体重支持を支援する制御を行う．

股関節の直立位維持支援として，股関節のアクチュエータに仮想的なバネ・ダンパ特性を与え，装着者の股関節を直立位に維持するために充分な弾性，粘性を関節に持たせる制御を行う．式(7)に股関節の支援トルク算出式を示す．

$$\tau_{spp\_h}=\tau_{bd\_h}=K_h(\theta_{abs\_ref}-\theta_{abs})-D_h\dot{\theta}_{abs} \quad (7)$$

ただし，τ_{spp_h} Nm は股関節の体重支持支援トルク，K_h は股関節ユニットのバネ定数，D_h は股関節ユニットのダンパ定数，θ_{abs} rad/sec は絶対角度の角速度，θ_{abs_ref} rad は絶対角度の目標角度である．

膝関節の伸展位維持支援として，股関節同様，膝関節のアクチュエータにも式(8)を用いて仮想的なバネ・ダンパ特性を与える．

$$\tau_{bd\_k}=K_k(\theta_{k\_ref}-\theta_k)-D_k\dot{\theta}_k \quad (8)$$

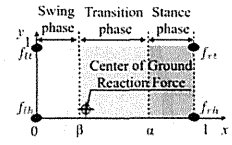

図4　右脚の歩行状態判定

Fig. 4　Walking phase determination of the right leg.

ただし，τ_{bd_k} Nm はバネ・ダンパ特性を持たせた膝関節支援トルク，k_k は膝関節のバネ定数，D_k は膝関節のダンパ定数，θ_{k_ref} rad は膝関節目標角度である．膝関節は支援期中の膝折れを抑制するため，膝関節の伸展位を維持するトルクとして τ_{lock} Nm を定め，式(9)に示した判別式によって膝関節の支持脚期支援制御で出力するトルクを決定する．

$$\tau_{spp\_k}=\begin{cases}\tau_{bd\_k}(|\tau_{bd\_k}|<|\tau_{lock}|)\\\tau_{lock}(|\tau_{bd\_k}|\geq|\tau_{lock}|)\end{cases} \quad (9)$$

ただし，τ_{spp_k} Nm は膝関節の体重支持支援トルクである．最終的な支持脚期支援制御トルク τ_{st} Nm は，式(10)に示すように支持脚期支援制御によって生成されたトルクと粘性摩擦補償トルクを組み合わせて生成する．

$$\tau_{spp}=\begin{bmatrix}\tau_{spp\_h}\\\tau_{spp\_k}\end{bmatrix}$$

$$\tau_{st}=\tau_{spp}+\tau_{Dcomp} \quad (10)$$

2·3·3　状態移行制御　提案する歩行支援手法は遊脚期と支持脚期の移行時に離散的となる系を連続したシステムとして扱う．したがって，各々の制御手法を連続的につなぐために，HALに備え付けられた足底荷重センサを用いて矢状面における床反力中心に基づいて歩行状態を遊脚期，支持脚期，状態移行期の3種類に判別する．

矢状面における床反力中心 C_x は，**図4**に示すように，左脚かかとを原点とし，右脚つま先が1となるように正規化を行う．式(11)に Cx の算出式を示す．

$$C_x=\frac{f_{rt}+f_{rh}}{f_{lt}+f_{lh}+f_{rt}+f_{rh}} \quad (11)$$

ただし，f_{rt} N は右つま先，f_{rh} N は右かかと，f_{lt} N は左つま先，f_{lh} N は左かかとの床反力である．

歩行状態の判別式は，右足が支持脚へ移行する値を α，遊脚へ移行する値を β として設定する．α と β の間を歩行状態の移行区間とし，式(12)を用いて支持脚期支援制御，遊脚期支援制御を混合させたトルク τ_{tr} Nm を出力する．

$$\tau_{tr}=\frac{C_x-\beta}{\alpha-\beta}\cdot\tau_{st}+\frac{\alpha-C_x}{\alpha-\beta}\cdot\tau_{sw} \quad (12)$$

2·4　HAL装着歩行試験

本試験では**図5**に示すHAL福祉用（CYBERDYNE社）を使用する．HAL福祉用は，HALの下肢モデルである

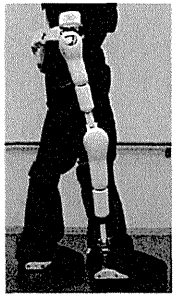

図5　ロボットスーツHAL

Fig. 5　Robot-Suit HAL.

HAL-5 Type-Cをベースに開発され，左右の股関節と膝関節の屈曲・伸展動作をアシストするアクチュエータを備えている．関節アクチュエータやBESセンサ，角度センサ，足底荷重センサなどの仕様は基本的にHAL-5 Type-Cと同じである[4]．HAL福祉用は足関節にアクチュエータを持たないため，試験協力者は短下肢装具により足関節を固定した上でHALを装着する．BESを計測する筋群は，事前試験と同様である．また，回転方向判定式の定数値は事前実験で確認した屈曲動作時及び，伸展動作時における屈筋BESの割合に基づいて決定する．遊脚期における弾性係数及び，粘性係数は，HALが中空において任意の姿勢維持が可能な値とする．支持脚期における弾性係数及び，粘性係数は，試験開始前に，装着者が平行棒とHALを用いて静止立位維持が可能となる値に調整する．状態移行制御に用いる α，β についても試験開始前に，患者の主観的な脚上げ意思とHALによる歩行状態判定結果の対応がつく値に調整する．

歩行試験開始時，試験協力者は平行棒内において免荷0 kgで立位となり，姿勢を安定させて待機する．歩行開始の指示と同時に歩行を開始し，可能な限り速く歩行を行う．各々の歩行周期に対する提案手法の有効性は，遊脚期においてBESと生成トルクを比較し，支持脚期において関節角度と生成トルクを比較することで確認する．また，平行棒内歩行3 mにおける歩行時間，歩数を計測し，歩行速度，歩幅，ケーデンスを求める．計測の際，前後1 mに助走距離，減速距離を設定する．HAL未装着時においても同様な試験を行い，比較を行う．

3.　結　　果

図6(a)にHAL未装着時の歩行姿勢，図6(b)にHAL装着時の歩行姿勢を示す．HAL未装着時には体幹が屈曲位になるが，HAL装着時は体幹が伸展位に維持されていることが確認できた．

図6　平行棒使用時の歩行姿勢
（a）HAL未装着時
（b）HAL装着時
Fig. 6　Gait using the parallel bars.
(a) Without HAL
(b) With HAL

図7に右股関節，右膝関節のBES，出力トルク，関節角度変化を示す．白色の領域は遊脚期，濃い灰色の領域は支持脚期，薄い灰色の領域は状態移行期である．股関節トルクは遊脚期においてBESの波形を反映しており，支持脚期において角度に依存した値が出力されていた．膝関節トルクは，6秒付近の遊脚初期において屈曲方向に出力され，8秒付近の遊脚終期で伸展方向に出力された．支持脚期では体重支持トルクが生成されており，膝関節角度を伸展位に維持できていた．

HAL装着時において平行棒内歩行3 mに要した歩数は21 steps，時間は1.83 minであった．よって，歩行速度は1.64 m/min，ケーデンス11.45 steps/min，ストライド長は0.143 mでの歩行を実現できることが確認できた．HAL未装着時は，平行棒内歩行が確認できなかった．試験協力者からは，「容易に腿上げができていると感じる．」「下肢で体重を支持しながら歩行していると感じる．」という感想が得られた．

4. 考　　察

遊脚期に生成されるトルクが，装着者が随意的に行う動作と同方向へ生成されていたことから，本提案手法によって試験協力者の遊脚期動作を支援できていたと考えられる．また，支持脚期中，股関節を直立位に維持し，膝関節を伸展位に維持できたことから，提案手法を用いることで試験協力者が単独での体重支持を実現できたと考えられる．したがって，本提案手法は矢状面における床反力中心に基づいて歩行状態の判別を行い，遊脚，支持脚を適切に支援できていたことが確認できた．

また，歩容評価の比較として，HAL未装着0 kg免荷状態における歩行試験を行ったが，歩行の計測が不可能であった．したがって，本提案手法によって，試験協力者の単独歩行を実現できたと言える．試験協力者が0 kg免荷状態での歩行を実現できたことから，本提案手法は単独での立位維持が困難な脳性麻痺患者に対する有効な歩行支援

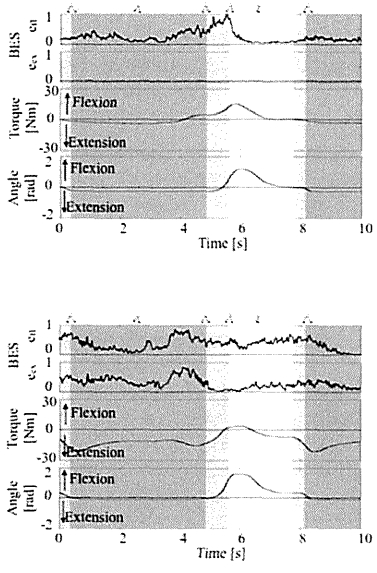

図7　平行棒内歩行時における正規化されたBES，出力トルク，関節角度
（a）右股関節
（b）右膝関節
Fig. 7　Normalized BES, output torque and joint angle while walking using the parallel bars.
(a) Right hip joint
(b) Right knee joint

手法となることが期待できる．

歩行中，試験協力者は下肢での体重支持を認識していた．したがって，下肢の体性感覚が刺激されていると考えられる．脳性麻痺患者の動作訓練において，適切な感覚刺激と運動活動の提示は，脳の可塑性に働きかけ運動機能を向上させる要素であり，運動活動の提示するロボットを用いた動作訓練によって粗大運動能力が向上した例も報告されている[6, 7]．そのため，HALを装着して歩行を繰り返し行うことで，未装着時における動作の改善も期待できる．

脳性麻痺の特徴は多種多様である．そのような課題に対応するため，複数の試験協力者への適用試験を行うことで症状の共通点と個別に対応すべき点を確認する必要があると考える．

本研究で提案した制御手法は日常動作へ対象動作を拡張することが可能と考えている．しかしながら，現在のシステムでは装着に介助が必要となる．したがって，動作支援

手法だけでなく単独での装着を実現する技術を開発し，脳性麻痺患者全体の支援システムへ発展させていく．

5. ま　と　め

本研究ではロボットスーツHALによる脳性麻痺患者の歩行支援手法を実現するため，単独での歩行が不可能な脳性麻痺患者1名を対象とした随意的動作支援手法と，HALが自律的に歩行姿勢を管理する制御手法を混在させた歩行支援手法を提案し，実証試験を通じて有効性を確認した．

本研究の成果により，自力移動が困難な脳性麻痺患者が本人の意思に基づく日常動作を実現し，車いすから離れて環境に依存せずに行動可能となることが期待される．

謝辞　本研究は，グローバルCOE：「サイバニクス」プログラムならびに，FIRST：「最先端人支援技術研究」プログラムの支援により行われた．また，JBMES2011においてベストリサーチアワードを受賞した．

文　　献

1. Krägeloh-Mann I, Cans C: Cerebral palsy update. Brain & development. **31**(7): 537-544, 2009.
2. Kawamoto H, Sankai Y: Power assist system HAL-3 for gait disorder person. in Proc. of the 2002 Int. Conf. on Computers Helping People with Special Needs (ICCHP 2002), Linz, pp. 196-203 (2002).
3. Lee S, Sankai Y: Power assist control for walking aid with HAL-3 based on EMG and impedance adjustment around knee joint. in Proc. of IEEE/RSJ Int. Conf. on Intel ligent Robots and Systems (IROS 2002), Lausanne, pp. 1499-1504 (2002).
4. Hayashi T, Kawamoto H, Sankai Y: Control method of RobotSuitHAL working as opeartor's muscleusing biological and dynamical information. Proc. of IEEE/RSJ Int. Conf. on Intelligent Robots and Systems, 2-6, Aug., (2005), pp. 3455-3460.
5. Jacquelin P, 武田功・弓岡光徳ほか監訳. 歩行分析―正常歩行と異常歩行. 医歯薬出版株式会社 (2007).
6. Meyer-Heim A, Borggraefe I, Ammann-Reiffer C, Berweck S, Sennhauser FH, Colombo G, et al.: Feasibility of robotic-assisted locomotor training in children with central gait impairment. Dev Med Child Neurol. **49**: 900-906, 2007.
7. Borggrafe I, Meyer-Heim A, Kumar A, Simon Schafer J, Berweck S, Heinen F: Improved gait parameters after robotic-assisted locomotor treadmill therapy in 6-year old child with cerebral palsy. Mov Disor. **30**, **23**(2): 280-283, 2008.

武富　卓三（タケトミ　タクミ）
2011年筑波大学大学院博士前期課程修了．修士（工学）．現在，同博士後期課程に在学し，2011年文部科学省グローバルCOEプログラム「サイバニクス：人・機械・情報系の融合複合」SRA研究員．「内閣府最先端研究開発支援プログラム」（健康長寿社会を支える最先端人支援技術研究）に従事．特に，装着型ロボットによる脳性麻痺の動作支援に関する研究開発を行う．
IEEE Student Member.

山海　嘉之（サンカイ　ヨシユキ）
1987年筑波大学大学院工学研究科修了．工学博士．筑波大学機能工学系助教授，米国Baylor医科大学客員教授を経て，現在，筑波大学大学院システム情報系教授，サイバニクス研究センター長，内閣府最先端研究開発支援プログラム「健康長寿社会を支える最先端人支援技術研究プログラム」研究統括，サイバニクス国際教育拠点リーダ，人・機械・情報系の融合複合新領域「サイバニクス」を開拓し，ロボットスーツHAL，生理・運動・神経系のセンシング技術・研究を推進．
日本ロボット学会理事，日本栓子検出と治療学会学会長などを歴任．

生体医工学
50(1)：117-123, 2012

研　究

自力運動困難な麻痺患者に対するロボットスーツを用いた新しい随意運動訓練
—重度脊髄損傷患者への臨床適用—

林　知広*・岩月　幸一**・長谷川 真人*・田上　未来*・山海　嘉之***

A New Voluntary Exercise using Robot Suit for Patients Having Difficulty in Active Movement
—Clinical Application to Severe Paraplegic Patients—

Tomohiro HAYASHI,* Koichi IWATSUKI,** Masato HASEGAWA,* Miki TAGAMI,* Yoshiyuki SANKAI***

Abstract The importance of voluntary exercise and sensory input in rehabilitation training after spinal cord injury (SCI) or cerebrovascular disease has been demonstrated by recent studies. However, the voluntary exercise is an impossible task for severe paraplegic and hemiplegic patients who cannot move their lower limbs by themselves. The purpose of this study is to verify whether these patients can perform a new voluntary exercise by using a robot suit which generates walking motion in place of the wearer's paralyzed muscles by detecting their voluntary bioelectrical signals. Two severe SCI patients who can barely produce neuromuscular activation but cannot move their lower limb participated in this study. Experimental results demonstrated that the robot suit was able to detect their voluntary neuromuscular activities via bioelectrical signals and provide stepping and walking motion having appropriate temporal relationship with the voluntary activities. In addition, the proposed voluntary exercise using the robot suit can significantly promote neuromuscular activities of the target muscles more than passive exercise.

Keywords : robot suit, rehabilitation training, voluntary exercise, sensory input, spinal cord injury.

1. はじめに

脊髄損傷や脳血管障害後のリハビリテーション（以下，リハ）では，自力運動が困難であっても，廃用症候群を防いで予後の向上を図るためには可能な限り早期から離床して動かない手足を動かしていく早期リハが有効とされている[1-4]．

生体医工学シンポジウム 2011 発表（2011 年 9 月，長野）
2011 年 7 月 29 日受付，2011 年 11 月 5 日改訂，2011 年 12 月 15 日再改訂
Received July 29, 2011; revised November 5, 2011, December 15, 2011.
* CYBERDYNE 株式会社　つくば研究所
CYBERDYNE Inc., Tsukuba R & D center.
** 大阪大学大学院医学系研究科脳神経外科
Department of Neurosurgery, Osaka University Graduate School of Medicine
*** 筑波大学大学院システム情報工学研究科
Center for Cybernics Research, University of Tsukuba

脊髄損傷や脳血管障害患者の回復を促進する上で，随意運動および運動に伴う感覚入力の重要性が示されている[5-10]．自力運動が困難な場合の訓練としてはタスク指向の感覚刺激を与えるためのロボットを用いた歩行訓練法[11-14]があるが，随意的神経・筋活動から運動を生成して感覚入力を受け取るという，通常の随意運動のようなフィードバックループを構築することが難しい．

我々はロボットスーツ HAL（Hybrid Assistive Limb）を開発してきた[15-20]．HAL は装着型のロボットで，装着者と一体となり運動を行うことができる．HAL が患者の生体電気信号に基づいて麻痺のある運動機能を補助・補完することで，随意的神経・筋活動と運動に伴う求心性入力との間に適切な因果関係を構築できると考えられる．

そこで，本研究では，運動開始意思を検出して患者に代わって運動を実行するロボットスーツを用いることで，重度麻痺患者に対する新しい随意運動訓練の実現可能性を検証することを目的とする．特に，重度の不全対麻痺患者を対象として，感覚刺激が重要とされる歩行運動の中でも転倒の危険性が低い Body Weight Support（以下 BWS）訓練[10]を行う．

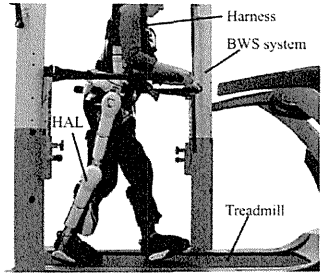

図 1　ロボットスーツ HAL-HT01A を使用した BWS トレッドミル歩行訓練の様子
Fig. 1　BWS treadmill walking with the robot suit HAL-HT01A.

2. 方　　法

2.1 ロボットスーツによるアシスト方法

本研究で用いたロボットスーツは**図 1** に示す HAL-HT01A（CYBERDYNE 社）である．HAL-HT01A は下肢用のロボットスーツで，左右の股関節と膝関節の屈曲・伸展動作をアシストするアクチュエータを備える．足関節については一般的な歩行訓練時と同様に，装具等を併用して底背屈中間位で固定した．

受傷後間もない時期などで自力運動が困難なほど重度の麻痺がある場合には，随意的な神経・筋活動を検出できる部位がごく一部に限られ，加えて痙性などの不随意的な筋活動を伴う可能性が高い．このような患者が歩行中の全ての神経・筋活動を自ら制御することは困難である．そこで，歩行に必要な神経・筋活動の中から患者が実現可能なものに的を絞って随意性を強化できる訓練法が必要となる．患者が行えない残りの動作については，ロボットスーツが代わりに実行・制御する必要があることから，その制御方法として，文献[20]に示す自律的制御法を用いた．本研究では，この制御法を用いるにあたり，より多様な筋から訓練対象を選べるように改良を加えた．

文献[20]の自律的制御法では，あらかじめ歩行フェイズごとに分割した運動パターンを用意し，ロボットスーツがフェイズを判断して各関節で実行する運動パターンを切り替える．歩行フェイズとしては「両脚支持期」，「左遊脚／右単脚支持期」，「右遊脚／左単脚支持期」の 3 つを定義した．両脚支持期から左右の遊脚／単脚支持期へ遷移するための随意的な神経・筋活動を検出し，それをトリガとして運動アシストのフェイズを切り替える（**図 2**）．また，遊脚／単脚支持期の終了条件すなわち両脚支持への遷移条件は，目標運動パターンが終端に到達することである．遊脚／単脚支持のアシスト中に遊脚／単脚支持への遷移条件を満たさなくなった場合でも，次の両脚支持の姿勢を作るように，目標パターンの終端まで動作を継続する．

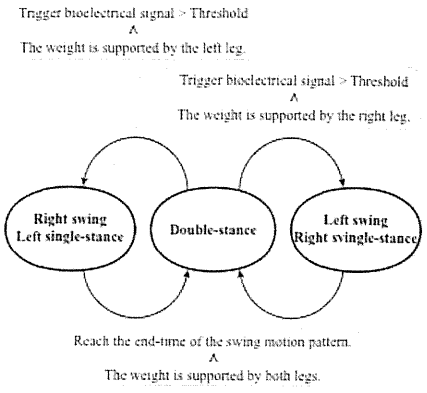

図 2　フェイズの遷移条件．トリガ生体電気信号の閾値はそれぞれの脚に対して設定される．
Fig. 2　Phase transition conditions. The thresholds for the trigger bioelectrical signals are determined for each leg.

随意的神経・筋活動を検出するため，左右の脚から随意性を訓練したい筋をそれぞれ一カ所選び，皮膚表面から得られた生体電気信号に平滑化処理をおこなったものをトリガ電位信号とする．両脚支持期においてトリガ電位信号が閾値を超えた時に遊脚／単脚支持期の運動パターンを開始する．

閾値は弛緩時の電位信号（以下，この基線をベースラインと呼ぶ）に対して設定する．閾値の大きさは装着者の随意的な信号変化量に応じて決める必要があるため，アシスト開始前に筋収縮を意識した時と弛緩した時の信号を計測し，装着者の主観的な筋収縮意思とロボットスーツによる判定結果の対応がつく値に調整する．また，ベースラインが運動訓練中に変動する可能性を考慮し，トリガ電位の長周期の変動を抽出する文献[20]の方法を用いてベースラインのオンライン推定も行う．

重度の麻痺がある場合には不随意的な神経・筋活動が見られる場合も多く，生体電気信号のみからでは遊脚の活動か支持脚の活動かを判断できない可能性もある．そこで，HAL が支持脚と遊脚を取り違えないように，足底荷重センサの情報から体重を支えている脚を判断する[20]．

従来筆者らが用いてきた手法では，トリガとして選べるのは遊脚側のみであったが，両脚期から遊脚／単脚支持期

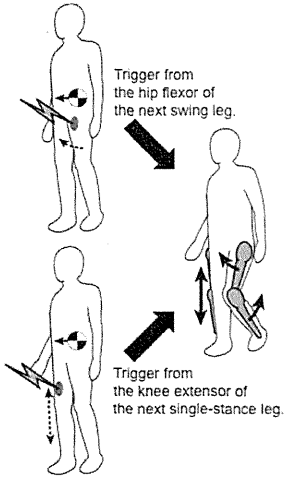

図3　トリガ信号と支持脚判定によるフェイズ遷移
Fig. 3　Phase transition based on the bioelectrical trigger signal and estimated stance limb.

に移行する際には，遊脚側は足の持ち上げ動作，支持脚側は膝折れ防止のための膝伸展動作を行う．そこで，本研究では，支持脚側の筋活動もトリガとして選択できるようにソフトウェアを改良した．それにより，**図3**に示す通り，遊脚の持ち上げをトリガとする場合には，(1)遊脚側のトリガ電位が閾値を超えている，(2)対側脚に体重が移行している，という二つの条件を同時に満たした時に同側の遊脚動作／対側の単脚支持動作を開始する．また，支持脚の膝伸展をトリガとする場合には，(1)トリガ電位が閾値を超えている，(2)同側脚に体重が移行している，という二つの条件を同時に満たした時に同側の単脚支持動作／対側の遊脚動作を開始する．

2·2　試験参加者と試験条件

本研究には2名の脊髄損傷患者（P1，P2）が参加した．P1は24歳男性で受傷部位はC5，受傷後2年の不全四肢麻痺であり，下肢の筋収縮は，わずかに触知できる程度で関節運動がみられなかった．試験参加時において，膝を伸ばそうと意識した際に，外側広筋から生体電気信号が検出可能であった．そこで，外側広筋の信号をトリガ生体電位とし，支持脚の膝伸展（膝折れ防止）を意識したときに，HALが同側の単脚支持／対側の遊脚フェイズ動作を開始するようにした．

P2は36歳男性で受傷部位はT7-T8，受傷後2年半であり，本試験参加の1年前に幹細胞移植手術の一つである自家嗅粘膜移植手術[21]を受けた．手術前は臨床的に完全対麻痺であり，本試験に参加した時点で下肢の関節運動を随意的に行うことは困難であった．試験参加時において，足を持ち上げようと意識した際に大腿二頭筋から生体電気信号が検出可能であった．そこで，大腿二頭筋の信号をトリガ生体電位とし，遊脚の持ち上げを意識したときに，HALが同側の遊脚／対側の単脚支持フェイズ動作を開始するようにした．

連続歩行を実現するためには，トリガに指定した筋の収縮から弛緩に要する時間と歩行周期が合うように，装着者の能力・状態に応じて目標パターンのパラメータを決める必要がある．そこで，随意的収縮を行ってから弛緩状態（ベースライン近傍）に戻るまでの時間を調べる予備試験を行った．その結果，P1については約3秒を要したため，単脚支持期（対側の遊脚期）を1.5秒に設定し，それに合わせてトレッドミル速度を0.4 km/hに設定した．P2はトリガの大腿二頭筋を一度収縮させると5秒以上持続してしまうことがあり，トレッドミルの最低速度でも収縮・弛緩の繰り返しが間に合わなかった．そこで，P2にはメトロノームで提示された音に合わせて交互に足を踏む足踏み動作を行ってもらうことにした．提示する時間間隔は，弛緩状態に戻るための十分な時間的余裕を設けるため9秒に設定した．また，遊脚期の時間はP1と同じく1.5秒とした．これ以上長くすると，単脚支持の姿勢維持に支障を来す恐れがあったためである．

提案する随意運動訓練を受動運動訓練と比較するため，以下の2つの条件の歩行動作を行った．

受動運動：フェイズ遷移の判定には生体電位トリガを用いない．HALは足底荷重センサから支持脚の切り替わり（体重移動）を検出してアシスト動作フェイズを切り替える．装着者は麻痺部の随意運動を特に意識しない．

随意運動：提案した随意運動訓練を行う．装着者はトリガとなる随意運動を意識する．

目標運動パターンやHALの制御パラメータは，随意運動と受動運動との間で同じ設定を用いた．

受動運動，随意運動それぞれでHALの動作に慣れるための練習を10分程度行った．その後，1試行あたり3分から5分を目安に連続歩行または足踏み運動を行った．それぞれの試行間には十分な休憩を挟んだ．

免荷量はHALのアクチュエータにより支持脚を維持できるように調整した．P1，P2ともにHALの重量を含めた全体重の40%に設定した．受動運動，随意運動を通して同じ免荷量とした．

なお，本研究は筑波大学の倫理委員会の承認をえた後，全ての試験参加者から書面にて同意を得て実施した．

2·3　比較評価方法

随意運動時には随意的な神経・筋活動が加わるため，受動運動時よりも信号が大きくなると考えられる．本研究では，受動運動と随意運動での神経・筋活動量を，以下の二点で比較した．

(a)　両脚支持期から遊脚／単脚支持期へ遷移した瞬間におけるトリガ電位信号，

(b)　遊脚／単脚支持期中のトリガ電位信号の積分値．

電位量の比較には，運動開始・停止時を除いた定常的な運動時の20歩分の計測値を用い，各試験参加者それぞれの脚について，Welch の T 検定を行った．有意水準は5%未満とした．

3.　結　　果

歩行時のトリガ電位信号の例として，P1の右脚から計測した信号の平均波形を**図4**に示す．受動運動時の電位信号は比較のために計測したもので，HALの制御には用いられなかった．

受動運動では単脚支持フェイズに切り替わりアシスト動作が開始されてから電位信号が上昇した（図4の矢印A）．一方，随意運動時にはフェイズが切り替わる前にトリガ電位が上昇した（図4の矢印B）．受動運動時には，装着者は下肢を随意的に動かそうと意識しなかったため，フェイズ切り替わり後にあらわれた生体電位の変化は，HALの運動に伴う感覚刺激により引き起こされた神経・筋活動を表していると考えられる．一方で随意運動時には積極的に麻痺部を動かそうと意識したため，HALのアシスト前に現れたトリガ電位の上昇は，随意的な神経・筋活動を反映したものと考えられる．

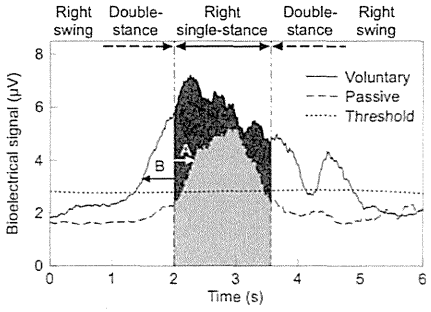

図4　トリガ電位信号の平均波形の例．P1の右脚から計測された20歩分の信号を平均したもの．受動運動では単脚支持期のアシスト動作が開始されてから電位信号が上昇した（矢印A）．一方で，随意運動ではフェイズが切り替わる前にトリガ電位が上昇した（矢印B）．
Fig. 4　Mean patterns of the trigger bioelectrical signal. These are calculated from 20 steps of the trigger signals measured from the right leg of P1. In the passive exercise, the bioelectrical signal was increased after starting the motion assistance for the single stance phase by the robot suit (Arrow A). In contrast it was increased before starting the assistance in the new voluntary exercise (Arrow B).

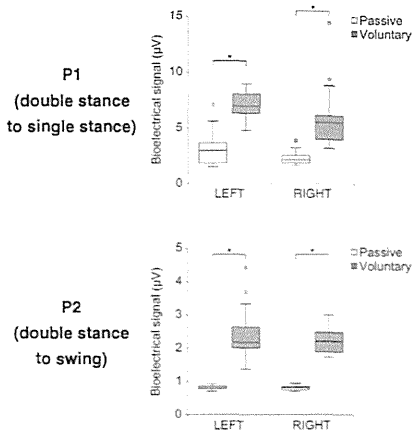

図5　両脚支持期からフェイズが切り替わった時刻のトリガ電位信号（$^*p < 0.01$，n = 20）．
Fig. 5　Boxplot of the trigger bioelectrical signals at phase shifting from the double-stance phase. $^*p < 0.01$, n = 20.

両脚支持期から遊脚／単脚支持期へ切り替わった時刻（図4の2秒の時点）のトリガ電位を**図5**に示す．P1，P2ともに随意運動時には電位が高くなっており，試験参加者それぞれの脚について，有意水準1%で統計的有意差が確認された．

さらに，アシスト動作中のトリガ電位の積分値（図4の網掛け部に相当）を**図6**に示す．全ての脚において，受動運動時よりも随意運動時の方が積分値が増加した（$p < 0.01$）．

4.　考　　察

随意運動時には，フェイズ遷移後のHALによる運動が開始される前にトリガ生体電位が上昇することが確認された．この上昇は受動運動時には見られず，トリガ対象部位の運動を意識したことで起きたものであり，随意的な神経・筋活動を反映したものと考えられる．この上昇分をトリガとして歩行運動をアシストできたことから，自力運動困難な患者であってもロボットスーツを用いることで随意的な神経・筋活動を反映した歩行または足踏み運動が実現可能であることが確認された．

さらに，トリガ検知の瞬間だけでなく，その後の動作

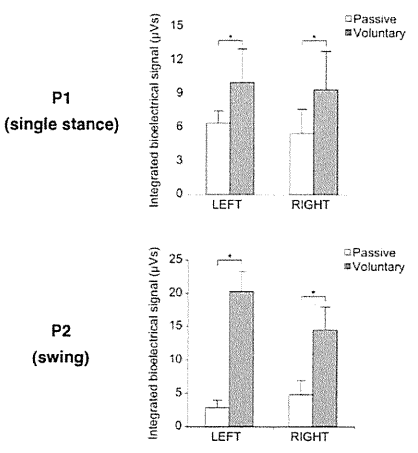

図6　随意運動の対象フェイズにおけるトリガ電位信号の積分値．P1は単脚支持期，P2は遊脚期を対象とした．エラーバーは標準偏差を表す（*$p < 0.01$, $n = 20$）．

Fig. 6　Integrated bioelectrical signals during the swing phase (P1) or the single-stance phase (P2). Error bars indicate standard deviations. *$p < 0.01$, $n = 20$.

フェイズ中においても，随意運動の方が受動運動よりも神経・筋活動量が増大した．これは，ロボットスーツが生成する運動により随意性の神経・筋活動と同期した求心性の神経刺激が得られ，筋・神経系の活動が促進されたものと考えられる．随意的神経・筋活動をトリガとしてロボットスーツが運動を生成することにより，受動訓練を行うよりも筋・神経系を効果的に賦活できる可能性が示されたことは，ニューロリハビリテーションの発展の観点からも意義がある．今後は，提案した随意運動訓練を継続した場合の運動機能の回復を定量的に評価することが重要である．

本研究で示した運動訓練はロボットスーツが関節運動を制御することにより運動パターンを生成可能であるため，下肢の自力運動が困難，あるいは部分的に運動を行えるが筋力の微調整が困難な患者が対象となる．ロボットスーツの制御方法には自律的制御手法の他に，患者の生体電気信号に基づき関節の動きそのものを制御する随意的制御手法があり[16, 19]，両者を組み合わせて用いることが可能である．患者が部分的にでも筋力の調整能力を獲得できれば，段階的に随意的制御手法に置き換えることで，難易度の高い訓練に移行できると考えられる．

また，脳血管障害後の片麻痺の場合は，非麻痺側の運動機能は比較的良好であるため，麻痺側に本研究で用いた生体電位トリガに基づく制御手法を用い，非麻痺側に随意的制御手法を用いることで，歩行訓練が可能になると考えられる．今後，片麻痺者についても，生体電位トリガを用いた運動訓練により筋・神経系を賦活可能であるかを検証する予定である．

最後に，自力運動困難な患者に対するロボットスーツを用いた運動訓練の安全性について述べる．運動機能が不十分な患者に対する歩行訓練では十分な安全性を確保する必要があるが，免荷装置の使用を前提とすることで立位姿勢に伴う転倒の危険性を極めて小さくできる．また，麻痺後に立位をとる際に考慮が必要となる起立性低血圧などについては，現在実施されている早期リハと同様に専門医等による病態管理・健康管理を行うことで安全性を確保可能である．実際に，本研究で実施した運動試験を通して有害事象は特に認められなかった．また，トレッドミルおよびHALの緊急停止を要するような事象も起きなかった．以上より，提案した歩行訓練方法は安全性の面からも実際の医療現場での実現性・有用性が十分に見込まれる．

5. ま　と　め

本研究では，自力運動が困難な重度脊髄損傷患者に対する新しい随意運動訓練を実現するため，麻痺部の不十分な生体電気信号から運動開始意思を検出して患者に代わって運動を行うロボットスーツを用いた歩行訓練試験を実施した．重度脊髄損傷者2名による歩行訓練試験において，自力運動困難な重度麻痺患者がロボットスーツを用いることで随意的な神経・筋活動と同期した歩行・足踏み運動を実施可能であることが確認された．また，随意性を伴わない受動運動訓練時と比較すると，提案した随意運動を行うことで訓練対象の筋・神経系を効果的に賦活可能であることが示された．次の課題として提案した随意運動による運動機能回復効果の定量的評価を行う予定である．

謝辞　本研究の一部は，内閣府最先端研究開発支援プログラム「健康長寿社会を支える最先端人支援技術研究プログラム」の支援により行われたものである．

文　献

1. Sumida M, Fujimoto M, Tokuhiro A, Tominaga T, Magara A, Uchida R: Early rehabilitation effect for traumatic spinal cord injury. Arch Phys Med Rehabil. **82** (3): 391-395, 2001.
2. Scivoletto G, Morganti B, Molinari M: Early versus delayed inpatient spinal cord injury rehabilitation: an Italian study. Arch Phys Med Rehabil. **86** (3): 512-516, 2005.
3. Musicco M, Emberti L, Nappi G, Caltagirone C: Early and long-term outcome of rehabilitation in stroke patients: the role of patient characteristics, time of initiation, and duration of interventions. Arch Phys Med Rehabil. **84** (4): 551-558, 2003.
4. Bernhardt J, Dewey H, Thrift A, Collier J, Donnan G: A very early rehabilitation trial for stroke (AVERT): phase II safety and feasibility. Stroke. **39** (2): 390-396, 2008.
5. Lotze M: Motor learning elicited by voluntary drive. Brain. **126** (4): 866-872, 2003.
6. Gómez-Pinilla F, Ying Z, Roy RR, Molteni R, Edgerton VR: Voluntary exercise induces a BDNF-mediated mechanism that promotes neuroplasticity. J Neurophysiol. **88** (5): 2187-2195, 2002.
7. Saeki S, Matsushima Y, Hachisuka K: Cortical activation during robotic therapy for a severely affected arm in a chronic stroke patient: a case report. J UOEH. **30** (2): 159-165, 2008.
8. Harkema SJ, Hurley SL, Patel UK, Requejo PS, Dobkin BH, Edgerton VR: Human lumbosacral spinal cord interprets loading during stepping. J Neurophysiol. **77** (2): 797-811, 1997.
9. Colombo G, Dietz V, Müller R: Locomotor activity in spinal man: significance of afferent input from joint and load receptors. Brain. **125** (12): 2626-2634, 2002.
10. Behrman AL, Harkema SJ: Locomotor training after human spinal cord injury: a series of case studies. Phys Ther. **80** (7): 688-700, 2000.
11. Colombo G, Joerg M, Schreier R, Dietz V: Treadmill training of paraplegic patients using a robotic orthosis. J Rehabil Res Dev. **37** (6): 693-700, 2000.
12. Reinkensmeyer DJ, Aoyagi D, Emken JL, Galvez JA, Ichinose W, Kerdanyan G, Maneekobkunwong S, Minakata K, Nessler JA, Weber R, Roy RR, Leon RD, Bobrow JE, Harkema SJ, Edgerton VR: Tools for understanding and optimizing robotic gait training. J Rehabil Res Dev. **43** (5): 657-670, 2006.
13. Veneman JF, Kruidhof R, Hekman EE, Ekkelenkamp R, Van Asseldonk EH, van der Kooij H: Design and evaluation of the LOPES exoskeleton robot for interactive gait rehabilitation. IEEE Trans Neural Syst Rehabil Eng. **15** (3): 379-386, 2007.
14. Banala SK, Kim SH, Agrawal SK, Scholz JP: Robot assisted gait training with active leg exoskeleton (ALEX). IEEE Trans Neural Syst Rehabil Eng. **17** (1): 2-8, 2009.
15. Okamura J, Tanaka H, Sankai Y: EMG-based prototype powered assistive system for walking aid. in Proc. Asian Symposium on Industrial Automation and Robotics, Bangkok, Thailand, pp. 229-234, 1999.
16. Nakai T, Lee S, Kawamoto H, Sankai Y: Development of power assistive leg for walking aid using myoelectricity and linux. in Proc. Asian Symposium on Industrial Automation and Robotics, Bangkok, Thai. pp. 295-299, 2001.
17. Suzuki K, Mito G, Kawamoto H, Hasegawa Y, Sankai Y: Intention-based walking support for paraplegia patients with robot suit HAL. Adv Rob. **21** (12): 1441-1469, 2007.
18. Eguchi K, Kawamoto H, Hayashi T, Sankai Y, Yoshida T, Shimizu T, Ochiai N: Use of a wearable robot—the hybrid assistive Limb—to assist walking in a stroke patient: a case report. Proceedings of the 5th world congress of the ISPRM, pp. 27-29, 2009.
19. Hayashi T, Kawamoto H, Sankai Y: Control method of robot suit HAL working as opeartor's muscle using biological and dynamical information. in Proc. International Conference on Intelligent Robots and Systems 2005, 2-6 Aug., pp. 3455-3460, 2005.
20. 林知広，岩月幸一，山海嘉之：神経・筋活動の制御に支障がある重度対麻痺患者の脚上げ意思推定と歩行アシスト．日本機械学会論文集C編．**77** (774): 439-449, 2011.
21. Lima C, Escada P, Pratas-vital J, Branco C, Arcangeli CA, Lazzeri G, Alberto C, Maia S, Capucho C, Hasse-ferreira A, Peduzzi JD: Olfactory mucosal autografts and rehabilitation for chronic rraumatic spinal cord injury. Neurorehabil Neural Repair. **24** (1): 10-22, 2010.

林　知広（ハヤシ　トモヒロ）

2002年筑波大学大学院修士課程理工学研究科修了，2010年同大学大学院博士課程システム情報工学研究科単位取得退学．修士（工学）．2007年よりCYBERDYNE株式会社研究員．ロボットスーツ，運動訓練支援システム，人間-ロボット協調技術などに関する研究開発に従事．2005年IEEE RAS Japan Chapter Young Award受賞．

IEEE，日本機械学会，計測自動制御学会の会員．

岩月　幸一（イワツキ　コウイチ）

1988年徳島大学医学部医学科卒業．医学博士．茨木医誠会病院脳神経外科部長等を経て，現在，大阪大学大学院医学系研究科脳神経外科講師，筑波大学大学院システム情報系客員准教授．ポルトガル共和国エガスモニツ病院にて臨床研修後，脊髄損傷患者に対して我国初の自家嗅粘膜移植を実施．

日本脳神経外科学会・専門医および評議員．日本脊髄外科学会・指導医．日本レーザー医学会監事・会誌編集委員．日本脳神経外科コングレス運営委員・プログラム委員．

長谷川　真人（ハセガワ　マサト）

2010年ボストン大学理学療法学科理学療法博士課程修了．理学療法士．東京大学医学部附属病院勤務を経て，2010年CYBERDYNE株式会社に入職，CYBERDYNE STUDIO責任者（研究員兼任）として，同施設内のトレーニング施設HAL FITにてロボットスーツHALの運用方法開発に従事する．専門領域は，神経系リハビリテーション，老年学，介護予防，理学療法管理学，セラピューティックレクリエーション学など．

日本理学療法士協会会員兼国際部協力部員．American Physical Therapy Association正会員．

田上　未来（タガミ　ミキ）

2010年茨城県立医療大学大学院保健医療科学研究科博士前期課程修了．理学療法修士．2010年博士後期課程に入学し現在に至る．2010年より財団法人茨城県科学技術振興財団「生活支援ロボット研究推進事業」において茨城県立医療大学プロジェクトメンバーとして研究に従事する．同年，CYBERDYNE株式会社に入職，トレーニング施設HAL FITにおいてHALを用いたトレーニングに従事する（研究員兼任）．専門領域は，内部障害理学療法学，基礎理学療法学．

理学療法士協会会員．呼吸ケア・リハビリテーション学会会員．心臓リハビリテーション学会会員．

山海　嘉之（サンカイ　ヨシユキ）

1987年筑波大学大学院工学研究科修了．工学博士．筑波大学機能工学系助教授，米国Baylor医科大学客員教授を経て，現在，筑波大学大学院システム情報系教授，サイバニクス研究センター長．内閣府最先端研究開発支援プログラム「健康長寿社会を支える最先端人支援技術研究プログラム」研究統括，サイバニクス国際教育拠点リーダ．人・機械・情報系の融合複合新領域「サイバニクス」を開拓し，ロボットスーツHAL，生理・運動・神経系のセンシング技術・研究を推進．

日本ロボット学会理事，日本栓子検出と治療学会学会長などを歴任．

電気学会論文誌 E（センサ・マイクロマシン部門誌）
IEEJ Transactions on Sensors and Micromachines
Vol.133 No.3 pp.57-65 DOI: 10.1541/ieejsms.133.57

Paper

Development of Hybrid Resistive-Capacitive Electrodes for Electroencephalograms and Electrooculograms

Alexsandr Igorevitch Ianov*a) Student Member, Hiroaki Kawamoto* Non-member
Yoshiyuki Sankai* Non-member

(Manuscript received June 21, 2012, revised Aug. 10, 2012)

Bioelectrical signals such as electrooculograms (EOGs) and electroencephalograms (EEGs) have many medical applications. Wet electrodes are used widely to acquire these signals; however, their use has several limitations. Other researchers have proposed dry contact electrodes, but they do not solve all of the problems associated with wet electrodes; on the other hand noncontact capacitive coupling electrodes have poor noise performance and are large and complex. In this paper, we present a hybrid electrode that is capable of both capacitive and resistive recordings at lower noise levels, with a smaller hardware footprint. The sensor was designed by optimizing the sensor input impedance value using a new electrode equivalent circuit that contained noise sources. Experiments were performed to investigate the frequency response, noise spectrum, motion artifacts, standard alpha and beta EEG signals, and eyelid and eyeball EOG measurements. We verified that our electrodes are capable of bioelectrical measurements at noise levels comparable to wet electrodes.

Keywords : bioelectrical sensing, capacitive sensing, electrode, EEG, EOG

1. Introduction

Bioelectrical signals that originate from the brain activity, such as electroencephalogram (EEG) signals, and those that originate from the eye movement, such as the electrooculogram (EOG) signals, are very important in several fields of medicine[1)-6)]. Wet resistive electrodes such as the Vitrode (Nihonkohden, Japan) or the electrodes used in the G.Tec electrode cap (G.Tec Medical Engineering GMBH, Austria) are used widely to perform these measurements. However, the use of wet electrodes has major drawbacks such as the requirement for skin preparation and the use of conductive gels[7)]. Dry resistive electrodes have been developed to increase sensor performance and usability[8)9)]. Dry electrodes involve an active resistive contact with the user's skin, which eliminates the need to use a gel and the problems associated with its use. Skin preparations such as body hair removal and cleaning may be required because constant electromechanical skin contact remains a requirement.

By contrast, noncontact electrodes have been proposed that are capable of achieving capacitive coupling between the electrode lead and the user's skin, thereby removing the need for skin preparation and electromechanical contact with the skin, which facilitates high usability[10)-14)]. However, ultra-high input impedances (10^{16}–10^{18} Ω) are required by the design. The ultra-high impedance input is highly susceptible to any electrostatic noise that originates from the surroundings. Therefore, robust shielding, isolation, and current leakage prevention techniques are required to reduce the noise. Furthermore, complex low noise bootstrapping techniques are required to avoid drift due to the bias current from the input. These disadvantages indicate that capacitive electrodes are considerably larger, noisier, and more expensive than conventional electrodes.

Daily life bioelectrical monitoring requires a sensor that gives the potentially high usability of capacitive coupling electrodes while retaining the high sensor performance of conventional electrodes. Our research is focused on the development of a novel sensing method that is capable of recording bioelectrical signals in both a resistive contact mode and a capacitive coupling mode at similar noise levels to commercially available electrodes. Previous studies only considered human body-electrode coupling in their designs, which maximized the input impedance. We also propose the use of noise source coupling in the sensor model. This model allows us to optimize the electrode impedance so that it is sufficiently high to record bioelectrical signals but low enough to reject external electrical noise, as required.

The aim of this study was to develop a novel electrode that combined the capabilities of both the capacitive and the resistive electrodes by optimizing the electrode input impedance using an original sensor equivalent circuit. Our electrode had to maintain a low noise characteristic that was comparable to commercially available wet electrodes during EEG and EOG measurements. Our electrode also needed to be small enough for high-resolution EEG recordings but easier to use than conventional electrodes.

First, we designed a novel sensor circuit model based on the consideration of the electronic components and the subject, which also accounted for the noise sources and their capacitive couplings with the system. Using this model, we developed an optimal original hybrid electrode that was capable of resistive contact and capacitive coupling sensing with an input impedance of 1 TΩ, which is about 10^4–10^6 times smaller than that proposed in other studies[11)-13)]. After optimizing the system, the circuit complexity was significantly reduced and the size of the sensor was minimized. This also allowed us to build the first portable 128-channel high-resolution EEG headset based on capacitive coupling electrodes. We collected the frequency response, noise spectrum, motion artifacts, and EEG and EOG bioelectrical data using our electrodes, which we compared with commercial electrodes. The results showed that our original hybrid electrodes had a similar noise spectrum to commercial electrodes and a lower noise spectrum than the electrodes proposed in other studies. They were also capable of recording signals with a correlation coefficient of >0.8 in the resistive contact and capacitive coupling modes.

2. Sensing Method Theory

We designed our hybrid resistive capacitive electrode such that it could function as a resistive contact electrode if electromechanical contact with the skin was not possible. Thus, the electrode collected bioelectrical signals via capacitive coupling if electromechanical contact was not possible. Capacitive sensing measures bioelectrical signals using the AC coupling between the electrode lead and the skin. Figure 1 shows the equivalent circuit for our proposed electrode containing a human body, the electrode-skin signal collection interface, the electrode circuit, and noise sources. The total electrical current in the electrode input is given by equation (1) as the sum of the currents from the noise sources and the current from the bioelectrical signal, i.e.,

$$\frac{V_{in}}{R_c} = \frac{(V_{nc}-V_{in})}{Z_{nc}} + \frac{(V_{nsei}-V_{in})}{Z_{nsei}} + \frac{(V_{bes}-V_{in})}{Z_{sei}} \quad \cdots\cdots (1)$$

where V_{bes} is the bioelectrical signal voltage, V_{in} is the electrode input voltage, V_{nsei} is the total noise source voltage at the skin-electrode surface, V_{nc} is the total noise source voltage on the electrode board, Z_{sei} is the skin-electrode interface impedance, R_c is the electrode input impedance, Z_{nsei} is the noise input impedance at the skin-electrode interface, and Z_{nc} is the noise input impedance on the electrode board. We can assume that the values for Z_{sei}, Z_{nsei}, and Z_{nc} are very large; therefore, we can simplify equation (1) as

$$V_{IN} = \frac{R_c}{Z_{nc}}V_{nc} + \frac{R_c}{Z_{nsei}}V_{nsei} + \frac{R_c}{Z_{sei}}V_{BES} \quad \cdots\cdots (2)$$

where Z_{sei} is represented as

$$Z_{sei} = (R_{sei}^{-1} + C_{sei}2\pi f)^{-1} \quad \cdots\cdots (3)$$

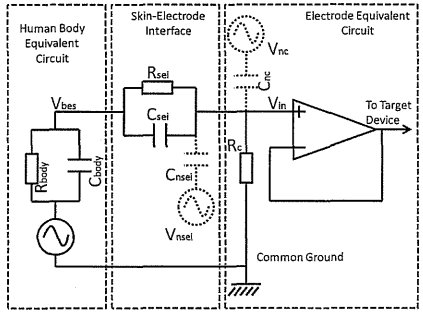

Fig. 1. Resistive-Capacitive Hybrid Electrode Equivalent Circuit

where C_{sei} is the capacitance, R_{sei} is the resistance between the electrode and the skin, and f is the signal frequency.

From equation (2) and (3), we can infer that the collected signal is highly dependent on the impedance of the electrode-skin interface and the total input impedance of the circuit, while the input impedance of the electrode should be considerably higher than the impedance at the electrode-skin interface. When our electrode is in the resistive contact mode, $C_{sei} \to 0$ so Z_{sei} is highly dependent on R_{sei}. When our electrode is in the capacitive coupling mode, however, $R_{sei} \to \infty$ so Z_{sei} is highly dependent on C_{sei}. From equation (3), we may assume the presence of noise sources in the surroundings that are connected via capacitive coupling to the input of the circuit. The impedance between the noise source and the electrode input is usually much higher than the impedance of the electrode-skin interface. Therefore, signals from the electrostatic noise sources may be amplified as well as or better than the bioelectrical signals if the electrode input impedance is excessively high. The effects of noise on the ultra-high impedance input may be strong if the electrode makes recordings using capacitive coupling sensing because Z_{sei} is already very high. Therefore, the input impedance should be set to a minimal value, which is sufficiently high to allow bioelectrical signals to be recorded.

A common ground signal between the body and the circuit is produced using a low impedance interface, such as that found in conventional electrode systems. Better signal noise ratios are obtained by maintaining a robust resistive ground[14)15)].

3. Hardware

3.1 Electrode Design To measure the EEG and EOG signals used by medical applications, our electrode needed to measure signals with frequencies ranging from 3 Hz to 100 Hz[16)17)]. The capacitive coupling mode requires a higher impedance than the resistive contact mode; therefore, the minimal circuit input impedance requirement is the input impedance used for the capacitive coupling measurements.

The capacitance of the skin-electrode interface in the capacitive coupling mode is given as

$$C_{sei} = \varepsilon_r \varepsilon_0 \frac{A}{d} \quad \cdots\cdots (4)$$

where ε_0 is the dielectric constant in vacuum, ε_r is the relative dielectric constant to the material, A is the electrode lead area nearest to the skin, and d is the distance between the skin and the electrode lead. As discussed in the previous section, we do not need to calculate the noise signal components in equation (2) because setting the input impedance at a minimal value also allows us to perform noise signal minimization. Given that $R_{sei} \to \infty$ in the capacitive coupling mode and by inserting combining equations (2), (3), and (4), we define the circuit input impedance as follows (5).

$$R_c = \frac{V_{IN}}{V_{BES}} \cdot \frac{d}{\varepsilon_r \varepsilon_0 A 2\pi f} \quad \cdots\cdots (5)$$

In the capacitive mode and based on the equivalent circuit described in Fig. 1, our electrode is a first-order high-pass filter with a theoretical cut-off frequency that is derived as follows:

$$F_{cut-off} = \frac{1}{2\pi R C_{sei}} \quad \cdots\cdots (6)$$

a) Correspondence to: Alexsandr Igorevitch Ianov. E-mail: ianov@golem.kz.tsukuba.ac.jp
* Graduate School of Systems and Information Engineering, University of Tsukuba
1-1-1, Tennoudai, Tsukuba 305-8573, Japan

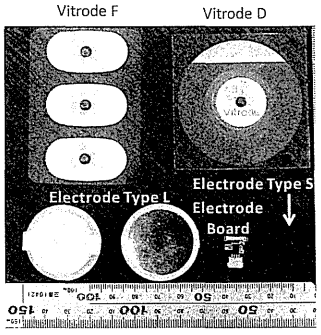

Fig. 2. Developed Electrodes and Vitrodes

where C_{sei} can be calculated from equation (4), and R is the input impedance of the operational amplifier used in the electrode design.

In this study, we developed two form factors for our hybrid electrode. Our developed electrodes are shown in Fig. 2. Electrode Type L is a large electrode with a circular 30 mm diameter stainless steel lead, which was based on the Vitrode D design. Type L was designed for low-density sensor networks with maximum comfort in mind. Electrode Type S is a small electrode with two 4 mm^2 cooper leads, which was designed for high-density sensor networks. *Type S has the smallest electrode lead area, and hence,* it also has the lowest capacitance in the capacitive coupling mode. During the design of the preamplifier circuit board, therefore, we assume a minimal electrode lead area A of 8 mm^2. We want V_{in} to be as close as possible to V_{bes}; therefore, we assume that V_{in}/V_{bes} is 1. We also assume that ε_r is close to 1 because air is an insulator, which can be considered as the worst-case scenario. When designing an electrode to record signals with a minimal frequency of 3 Hz that works up to 1 mm from the skin in the capacitive coupling mode, we calculated that a minimal input impedance R_c of approximately 0.85 TΩ is required.

An instrumentation amplifier with an input impedance of 1.00 TΩ was used in the design of our electrode. An instrumentation amplifier was used because it offers a very reliable and easily configurable circuit in a single small package. The selected amplifier also had an input bias current of 10 pA. In the capacitive coupling mode, the bias current can produce an undesirable DC drift if a path is not available, which may even lead to signal distortion during long-term measurements. A bias current path was created using two back-to-back Schottky diodes, which were connected in series to a grounded resistor. This limited the offset to an absolute value of 0.13 V, which provided a path for the bias current while maintaining the input impedance value. The theoretical cutoff frequency calculated using formula (6) is 2.3 Hz.

3.2 Data Collection System The developed electrode data recording and evaluation system included three stages. In the first stage, a second instrumentation amplifier receives analog signals from two electrodes and outputs the amplified difference between them. The second stage is responsible for conditioning the signal for the AD converter. The second stage used an eighth-order Butterworth bandpass filter and a voltage level

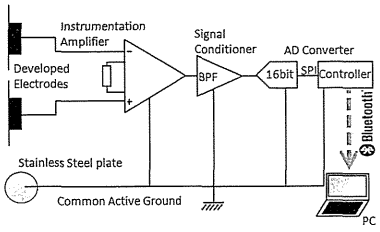

Fig. 3. Data Collection System Diagram

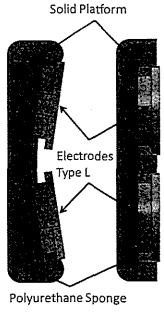

Fig. 4. Developed Electrodes and Vitrodes

converter. If necessary, the filter could be bypassed using a switch. The final stage involved a 16-bit AD converter connected via an SPI channel to a microcontroller. Signal sampling was performed at 4 kHz. Data was transferred from the controller to a laptop computer via a class-2 Bluetooth v3.0 connection using the Host-Controller Interface protocol. This system is compatible with the hybrid electrodes and the commercially available Vitrode electrodes for simultaneous comparative recordings. The common ground was connected to a clean exposed body area of the user via a stainless steel plate. Each sensor was connected to the system using a 1-m long cable. A block diagram of the data recording system is shown in Fig. 3.

A method for reducing motion artifacts due to head movements and external forces applied to the electrodes was used to increase the signal robustness. An electrode pair was mechanically coupled; therefore, the relative motion between the electrode pair records similar motion artifact signals as common mode noise. Common mode noise is cancelled by the differential amplifier in the first stage of the measurement system. The mechanical coupling structure for electrode Type L is shown in Fig. 4.

Headsets were developed for both types of electrodes. A headset for electrode Type L is shown in Fig. 5 (a), which uses the mechanical coupling structure shown in Fig. 4 to place electrodes on the user's head. The measured areas are above the frontal lobe of the brain to generate low-resolution EEG measurements and near the user's eyes for EOG measurements. A second headset was developed as a prototype for a portable high-spatial-resolution EEG recording system. The assembled headset used 128 Type S

(a) Low Spatial Resolution Type L Headset

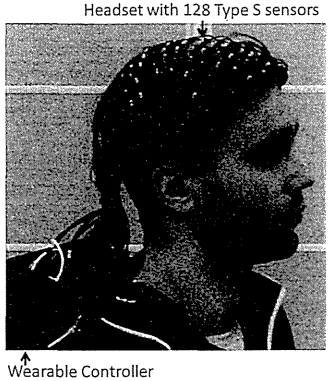

(b) 128 Channel High Spatial Resolution Type L Headset

Fig. 5. Developed headsets

electrodes, as shown in Fig. 5 (b).

4. Evaluation Experiments and Results

4.1 Frequency Response Evaluation In this experiment, we measured the frequency responses of our electrodes in the resistive contact mode and the capacitive coupling mode. The experimental setups are shown in Fig. 6. The electrode made direct contact with a metal signal plate attached to a function generator (WF1946B, NF Corporation, Japan) when measuring the resistive contact mode signals. To determine the capacitive mode responses, the electrode and the metal signal plate were separated by a 1 mm thick insulating rubber layer. The filters used in the data collection system shown in Fig. 3 were bypassed in this experiment to facilitate direct measurements of the electrode frequency responses.

Figure 7 shows the results for the Vitrode and the hybrid electrode in the resistive mode and capacitive mode, as well as the

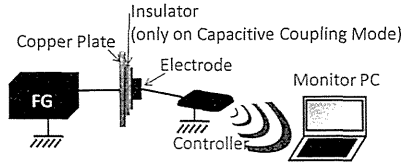

Fig. 6. Sensor Frequency Response Evaluation Experiment Set-up Diagram

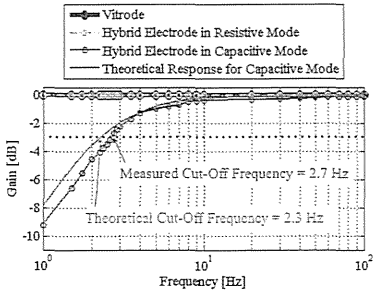

(a) Gain Frequency Response

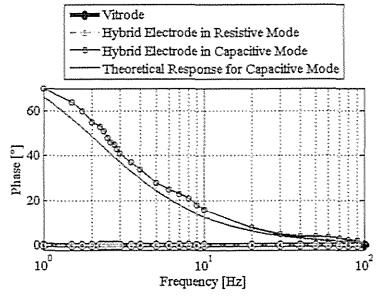

(b) Phase Frequency Response

Fig. 7. Frequency Response for the Developed Electrodes and Vitrode

theoretical frequency responses of the electrode in the capacitive mode. The results show that the frequency response of our electrode in the resistive mode was identical to that of Vitrode F. As both electrodes directly connect the substrate to the amplifier, there was no phase or gain change in the target frequency band.

Our results showed that the experimental cutoff frequency of 2.7 Hz was close to the theoretical cutoff frequency of 2.3 Hz. The results also showed that the hybrid electrode and the model behaved in a very similar manner to a first-order high-pass filter, as predicted by our model. The difference in the cutoff frequency was attributed to the assumptions of our model, which only considered the ideal electronic components of the system. When

developing the electrode, we added new resistive and capacitive features on the basis of the high-impedance input bias current escape path circuit described in Section 3.1 and the printed circuit board pattern and materials. The resultant input impedance was a combination of the amplifier input impedance and the impedance from the new elements. The difference in the input impedance created a difference in the cutoff frequency.

Our model was not a perfect representation of the entire system; however, 2.7 Hz was very close to the target cutoff frequency and it was an adequate value for applications in the 3–100 Hz band, which are discussed in this paper.

4.2 Electronic Noise Evaluation The noise levels attributable to the electronic sources of the electrode were measured by connecting the inputs of two electrodes. Resistive contact mode measurements were performed by directly shorting the inputs of the two electrodes. Capacitive coupling mode measurements were performed by placing the inputs face to face, separated by only a 1 mm thick insulating rubber layer. The experiment setup is shown in Fig. 8. The noise spectrum of the Vitrode F wet Ag/AgCl electrodes was also measured in a manner similar to that used for our electrodes in the resistive mode.

The noise spectrum obtained is shown in Fig. 9. The Vitrode and the hybrid electrode in the resistive mode had very similar

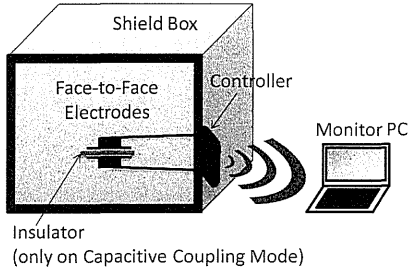

Fig. 8. Sensor Noise Spectrum Evaluation Experiment Set-up Diagram

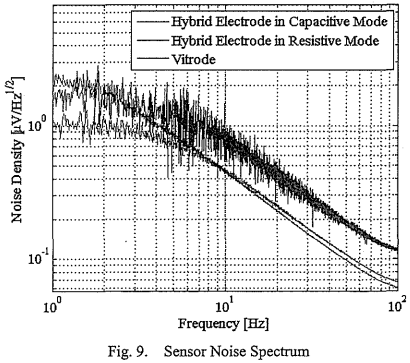

Fig. 9. Sensor Noise Spectrum

noise spectrum characteristics in the 10–100 Hz band because they were both resistive contact-type electrodes and they were electrically coupled better with the substrate than the environment. In the 1–10 Hz band, however, our hybrid electrodes had about 1 $\mu V/Hz^{1/2}$ less noise than the Vitrode because our electrode was an active, pre-amplified type of electrode whereas the Vitrode was a passive electrode[8][9].

Because the Vitrode F is a passive electrode, it was more susceptible to displacement currents due to chemical degradation of the Ag/AgCl gel and electrostatic effects in the 1-m-long cable that connected the electrode lead to the amplifier and the measurement system.

However, the hybrid electrode in the capacitive mode was about 0.3 and 1 $\mu V/Hz^{1/2}$ noisier than the other two cases. According to the model shown in Fig. 1 and equations (2) and (3), the relative value of the impedance value was lower in the capacitive mode when coupling the environmental noise sources (Z_{nc} and Z_{nsei}) compared with the impedance of the coupling with the signal source (Z_{sei}) in the resistive contact mode. This condition allowed the electrode to couple the environment noise sources better. However, our new optimal impedance electrode design indicated that the noise levels were at least two times smaller than the weakest bioelectrical signals considered in this study and 4–6 $\mu V/Hz^{1/2}$ smaller than the capacitive coupling electrodes proposed in other studies[13].

This low noise characteristic in the resistive and capacitive modes was comparable to that of conventional electrodes, and it showed that our electrode was a viable sensor for detecting EEG and EOG signals.

4.3 Motion Artifact Evaluation We evaluated the potential use of our electrodes in real-world applications and the effectiveness of the mechanical coupling method proposed in Session 3.2 by recording motion artifacts when the participant moved his head. In this experiment, the participant changed the pitch angle of the head by ±45° every 1 s for 10 s, before resting for another 10 s.

Recordings were made in the resistive contact and capacitive coupling modes with the Type L electrodes and Vitrode F electrodes using the headset shown in Fig. 5 (a). The Vitrode F electrodes were attached to the skin areas that had been cleaned with alcohol to remove any sweat and skin oils, in accordance with the manufacturer's instructions. Skin preparation was not required for our hybrid electrode in the resistive or capacitive modes. Resistive contact mode data were acquired when the developed electrodes were in direct contact with the skin of the participant. Capacitive coupling mode data were acquired when the developed electrode was isolated from the skin of the participant using a 1 mm thick insulating rubber layer. The electrodes were located in the EOG recording area of the headset. The data obtained are shown in Fig. 10. Our developed electrode produced no motion artifacts in the resistive contact or capacitive coupling modes, whereas the commercially available electrodes recorded spikes with every head movement.

Thus, the mechanical coupling of multiple electrodes eliminated the relative motion between them and contributed to eliminating the motion artifacts in recordings made by Vitrode electrodes, as reported in other studies[18]. Furthermore, the Vitrode electrodes still recorded motion artifacts even when they were mechanically coupled because Vitrode electrodes are passive wet electrodes. The signals transmitted through the cables from passive electrodes

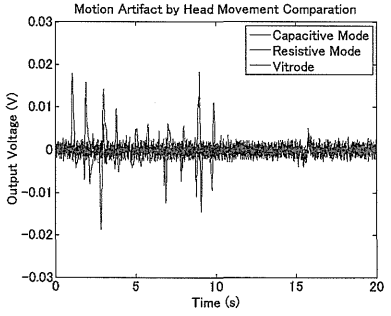

Fig. 10. Head-Motion Originated Motion Artifact Measurements

are high impedance signals that are susceptible to noise. During head movements, the Vitrode cables also moved and this affected the coupling configuration with the environment, which produced noise. By contrast, our electrodes output a buffered low impedance signal, which was robust against cable motion artifacts.

4.4 EOG Recording Experiments Eyeball and eyelid movement recordings were made using Type L electrodes in the resistive contact and capacitive coupling modes. The resistive contact and capacitive coupling mode recordings were made in a similar manner to the experiment described in Section 4.3. Simultaneous recordings with Vitrode F were made for comparative purposes. The Vitrode F electrode pair was positioned as close as possible to our developed electrodes, where the center of each Vitrode electrode was 30 mm from the center of the nearest developed electrode. The Vitrode F electrodes were attached to skin areas that had been cleaned with alcohol to remove any sweat and skin oils, in accordance with the manufacturer's instructions. No skin preparation was required for our hybrid electrode in the resistive or capacitive modes. However, the electrode was isolated from the skin using a 1-mm-thick rubber layer during the capacitive mode experiments.

Pearson's correlation coefficient ρ for the data collected from the hybrid electrode and Vitrode F was calculated as follows:

$$\rho = \frac{\sum_{i=0}^{n} X_i Y_i - \frac{\sum_{i=0}^{n} X_i \sum_{i=0}^{n} Y_i}{n}}{\sqrt{\left(\sum_{i=0}^{n} X_i^2 - \frac{\left(\sum_{i=0}^{n} X_i\right)^2}{n}\right)\left(\sum_{i=0}^{n} Y_i^2 - \frac{\left(\sum_{i=0}^{n} Y_i\right)^2}{n}\right)}} \quad \cdots\cdots (7)$$

where n is the number of samples, X_i is a sample from our hybrid electrode, and Y_i is a sample from the Vitrode F electrode.

During eyelid movement recordings, the participant blinked at a frequency of 1 Hz, according to a metronome. The datasets obtained are shown in Fig. 11. The calculated correlation coefficient for the data collected from our electrodes in the resistive contact mode and Vitrode F was 0.94, while the correlation coefficient for data collected from our electrodes in the capacitive coupling mode and Vitrode F was 0.92.

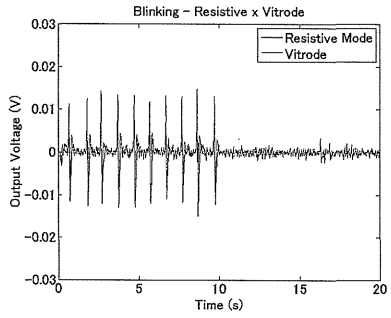

(a) Resistive Mode

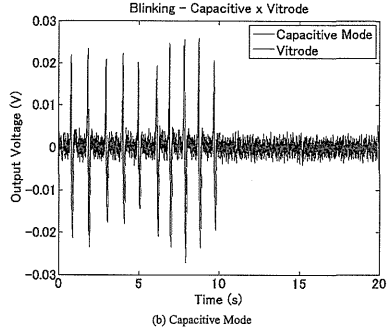

(b) Capacitive Mode

Fig. 11. Eyelid EOG Recordings

During eyeball movement recordings, the participant moved his eyeballs up and down at a frequency of 0.5 Hz, according to a metronome. The datasets obtained are shown in Fig. 12. The calculated correlation coefficient for the data collected from our electrodes in the resistive contact mode and Vitrode F was 0.95, while the correlation coefficient for the data collected from our electrodes in the capacitive coupling mode and the Vitrode F was 0.90.

4.5 Low Resolution EEG Recording Experiments The 10–20 Hz band bioelectrical signal recording capacity of our hybrid electrodes was tested by performing alpha and beta band EEG recording experiments. The three types of electrodes were placed over the skin, as described in Section 4.4. A pair of Type L electrodes was positioned, using the headset shown in Fig. 5, near the forehead and near points F3 and F4 in the International 10–20 Electrode Placement System[18]. The correlation coefficient for the data obtained using the hybrid electrode and the Vitrode was calculated using equation (7).

EEG signals were measured while the participant kept their eyes open for 30 s when beta waves were predominant, and they were then closed for another 30 s when the alpha waves were predominant. Figure 13 shows the spectrograms of the recorded data and a binary version that only shows signals >1 dBmV, for all three types of measurements. The spectrograms clearly show

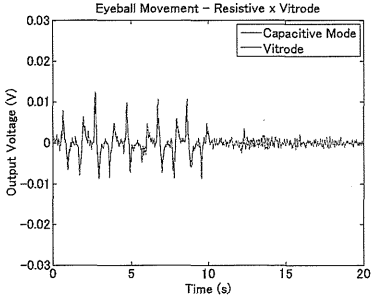

(a) Resistive Mode

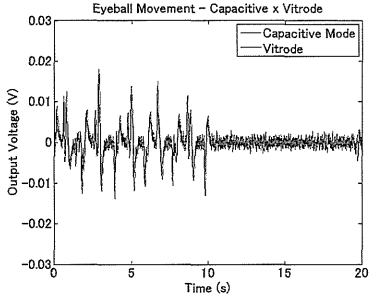

(b) Capacitive Mode

Fig. 12. Eyeball EOG Recordings

that our electrodes measured strong beta bands during the first 30 s and strong alpha bands during the last 30 s of the experiment. The calculated correlation coefficient for the data collected from our electrodes in the resistive contact mode and Vitrode F was 0.90, while the correlation coefficient for the data collected from our electrodes in the capacitive coupling mode and Vitrode F was 0.84. The results show that our Type L electrodes delivered a performance that was comparable to that of conventional electrodes when sensing EEG signals.

4.6 High Resolution EEG Recording Experiments

Using the high-resolution headset and Type S electrodes shown in Fig. 6, we repeated the experiments reported in Section 4.5. The observed electrode position and placement conditions were the same as those used in the previous section. Simultaneous readings were also performed using Vitrode electrodes, and the correlation coefficient between the data derived from the hybrid electrode and the Vitrode was calculated using equation (7).

The EEG recording protocols used in Section 4.5 were also used in this experiment. Figure 14 shows the spectrograms of the data collected using all three types of electrodes and binary versions for signals >1 dBmV. As in the previous experiment, the hybrid Type L electrode was also capable of recording strong beta band signals during the first 30 s of the experiment and strong alpha band signals during the second 30 s of the experiment. The calculated correlation coefficient for the data collected from our electrodes in the resistive contact mode and Vitrode F was 0.86, while the correlation coefficient for the data collected from our electrodes in the capacitive coupling mode and the Vitrode F was 0.85.

Alpha and beta waves were observed simultaneously in this and the previous experiment owing to the low noise design, which is the first time this has been achieved using capacitive coupling electrodes.

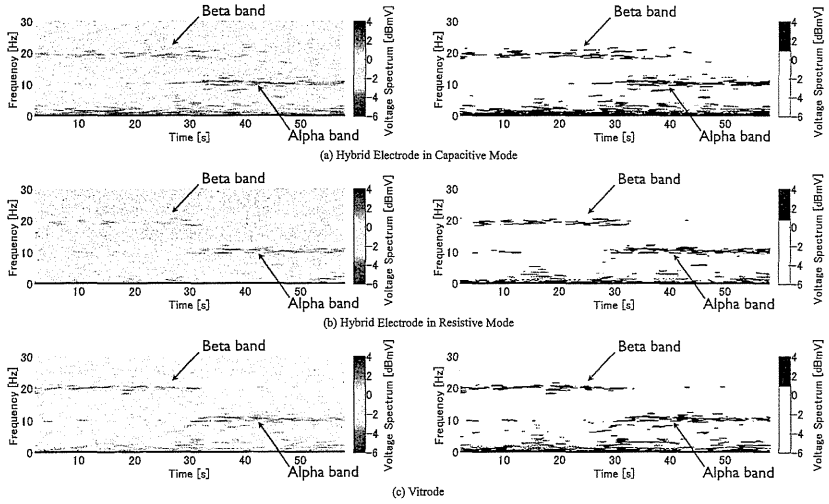

(a) Hybrid Electrode in Capacitive Mode

(b) Hybrid Electrode in Resistive Mode

(c) Vitrode

Fig. 13. EEG Recordings using Type L electrodes

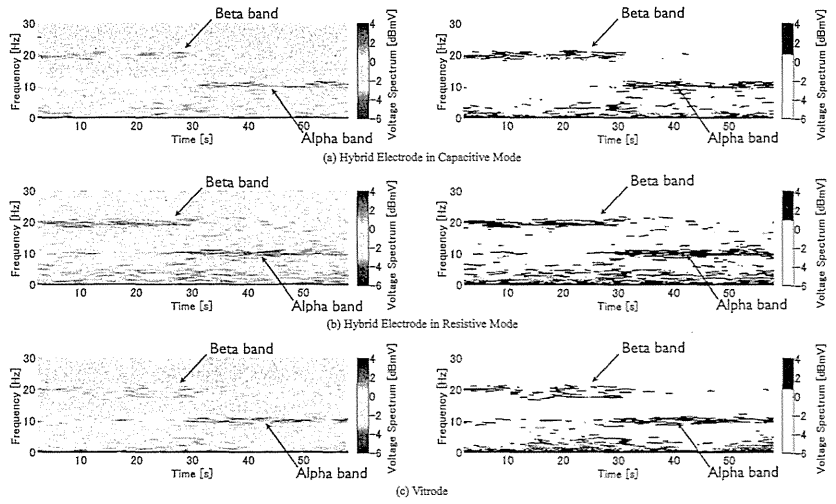

(a) Hybrid Electrode in Capacitive Mode

(b) Hybrid Electrode in Resistive Mode

(c) Vitrode

Fig. 14. EEG Recordings using Type S electrodes

5. Discussion

EOG and EEG signals are used extensively for sleep disorder diagnosis and treatment, assistive device control, and neurorehabilitation[1]-[6]. The effectiveness of some of these medical applications is highly dependent on the frequency at which the patient uses the equipment. One of the main obstacles in the spread of these technologies is the difficulty of placing electrodes and performing measurements during daily life because of the requirements for skin preparation and the electromechanical contact problems associated with conventional electrodes[7]-[9]. From a usability perspective, our electrodes are easier to use than any commercially available electrodes. As shown in Sections 4.3–4.6, skin preparation is unnecessary and our electrodes can even measure bioelectrical signals in covered body areas were electromechanical contact is impossible. Furthermore, future medical applications may require that patients regularly use high-resolution headsets and measurement devices similar to the one in Fig. 5, and devices equipped with our electrodes can be placed on in a fraction of the time of conventional devices. This high usability has the potential to increase reliability. If electrodes are easier to use, the probability of human error is reduced. This higher usability makes our electrodes a significant step toward the popularization of wearable sensors and computers during daily life.

The experimental results presented in Sections 4.1 and 4.2 support our electrode impedance optimization method and our optimal model in terms of its noise and frequency utility. The optimization results showed that the noise levels were 4–6 $\mu V/Hz^{1/2}$ lower than those reported by other studies. Our optimized design allowed us to develop an 8 mm^2 capacitive coupling electrode, which was four times smaller than electrodes developed in other studies. This smaller size allowed us to develop the first portable 128-channel high-resolution EEG headset based on capacitive coupling electrodes. The frequency response results were very close to the theoretical values; however, the observed difference suggested that the resulting input impedance in the actual electrode is slightly lower than the target value. This was not a problem for the applications described in this paper; however, some commercial and medical situations require very high levels of reliability or industrial standard definitions, so a full understanding of the electrode impedance may be required. An enhanced model that includes resistive and capacitive elements using additional board components and board design features, and different materials, may be introduced in future works.

The observed correlation coefficients for the EOG experiments presented in Section 4.3 were all above 0.90. However, the correlation coefficients in the EEG experiments in Sections 4.5 and 4.6 were between 0.84 and 0.90. The EEG readings had lower correlation coefficients because they were 10–100 times weaker than the EOG signals. Weaker signals had a larger effect on the random thermal noise shown in Fig. 9, which reduced the correlation between the two different readings. Another factor was the distance between the electrodes. Previous studies have shown that a 30-mm distance between the centers of the two electrodes during simultaneous recordings was sufficient to produce different signals[19] and a lower correlation.

6. Conclusion

In this study, we developed an electrode that combined the characteristics of capacitive and resistive electrodes by optimizing the electrode input impedance using an original sensor equivalent circuit. Our electrode maintained a low noise level that was comparable to the noise level maintained by commercially available wet electrodes during EEG and EOG measurements. Our electrode was small enough for high-resolution EEG recordings

and easier to use than conventional electrodes.

In future studies, we intend to increase the accuracy of our electrode model and expand the design to other bioelectrical signals. Our sensor will help increase the usability and reliability of electrodes and promote the popularization of medical and wearable devices in daily life.

Acknowledgement

Part of this work was supported by the "Funding Program for World-Leading Innovative R&D on Science and Technology (FIRST Program)," which was initiated by the Council for Science and Technology Policy (CSTP).

References

(1) M. L. Fantini, M. Michaud, N. Gosselin, G. Lavigne, and J. Montplaisir : "Periodic leg movements in REM sleep behavior disorder and related autonomic and EEG activation", Neurology, Vol.59, No.12, pp.1889-1894 (2002)

(2) R. M. Coleman, C. P. Pollak, and E. D. Weitzman : "Periodic movements in sleep (nocturnal myoclonus): Relation to sleep disorders", Annals of Neurology, Vol.8, No.4, pp.416-421 (1980)

(3) R. J. K. Jacob : "The use of eye movements in human-computer interaction techniques: what you look at is what you get", ACM Transactions on Information Systems (TOIS) - Special issue on computer human interaction, Vol.9, No.2, pp.152-169 (1991)

(4) J. K. Chapin, K. A. Moxon, R. S. Markowitz, and M. A. L. Nicolelis : "Real-time control of a robot arm using simultaneously recorded neurons in the motor cortex", Nature Neuroscience, Vol.2, pp.664-670 (1999)

(5) K. K. Ang, C. Guan, K. S. G. Chua, B. T. Ang, C. Kuah, C. Wang, K. S. Phua, Z. Y. Chin, and H. Zhang : "Clinical study of neurorehabilitation in stroke using EEG-based motor imagery brain-computer interface with robotic feedback", 2010 Annual International Conference of the IEEE Engineering in Medicine and Biology Society, pp.5549-5552 (2010)

(6) J. D. Allison, K. J. Meader, D. W. Loring, R. E. Figueroa, and J. C. Wright : "Functional MRI cerebral activation and deactivation during finger movement", Neurology, Vol.54, pp.135-142 (2000)

(7) J. R. Wolpaw, N. Birbaumer, W. J. Heetderks, D. J. McFarland, P. H. Peckham, G. Schalk, E. Donchin, L. A. Quatrano, C. J. Robinson, and T. M. Vaughan : "Brain-computer interface technology: a review of the first international meeting", IEEE Trans. Rehabilitation Engineering, Vol.8, No.2, pp.164-173 (2000)

(8) T. J. Sullivan, S. R. Deiss, T. P. Jung, and G. Cauwenberghs : "A brain-machine interface using dry-contact, low-noise EEG sensors", Proc. IEEE Int. Symp. Circuits and Systems, pp.1986-1989 (2008)

(9) G. Gargiulo, R. A. Calvo, P. Bifulco, M. Cesarelli, C. Jin, A. Mohamed, and A. V. Schaik : "A new EEG recording system for passive dry electrodes", Clinical Neurophysiology, Vol.121, No.5, pp.686-693 (2010)

(10) A. Lopez and P. C. Richardson : "Capacitive electrocardiographic and bioelectric electrodes", IEEE Trans. Biomedical Engineering, Vol.16, pp.299-300 (1969)

(11) C. J. Harland, T. D. Clark, and R. J. Prance : "Electric potential probes -new directions in the remote sensing of the human body", Measurement Science and Technology, Vol.2, pp.163-169 (2002)

(12) Y. M. Chi and G. Cauwenberghs : "Micropower non-contact EEG electrode with active common-mode noise suppression and input capacitance cancellation", Engineering in Medicine and Biology Society, pp.4218-4221 (2009)

(13) Y. M. Chi, T. P. Jung, and G. Cauwenberghs : "Dry-Contact and Noncontact Biopotential Electrodes: Methodological Review", IEEE Reviews in Biomedical Engineering, Vol.3, pp.106-119 (2010)

(14) J. Harland, T. D. Clark, and R. J. Prance : "Electrical potential probes - new directions in the remote sensing of the human body", Measurement Science and Technology, Vol.13, pp.163-169 (2002)

(15) M. J. Burke and D. T. Gleeson : "A micropower dry-electrode ECG preamplifier", IEEE Trans. Biomedical Engineering, Vol.47, No.2, pp.155-162 (2000)

(16) D. V. Moretti, F. Babiloni, F. Carducci, F. Cincotti, E. Remondini, P. M. Rossini, S. Salinari, and C. Babiloni : "Computerized processing of EEG-EOG-EMG artifacts for multi-centric studies in EEG oscillations and event-related potentials", International Journal of Psychophysiology, Vol.47, No.3, pp.199-216 (2003)

(17) J. C. Woestenburg, M. N. Verbaten, and J. L. Slangen : "The removal of the eye-movement artifact from the EEG by regression analysis in the frequency domain", Biological Psychology, Vol.16, No.1-2, pp.127-147 (1983)

(18) W. Klimesch, B. Schack, M. Schabus, M. Doppelmayr, W. Gruber, and P. Sauseng : "Phase-locked alpha and theta oscillations generate the P1?N1 complex and are related to memory performance", Cognitive Brain Research, Vol.19, No.3, pp.302-316 (2004)

(19) G. Rau and C. Disselhorst-Klug : "Principles of high-spatial-resolution surface EMG (HSR-EMG): single motor unit detection and application in the diagnosis of neuromuscular disorders", Journal of Electromyography and Kinesiology, Vol.7, No.4, pp.233-239 (1997)

Alexsandr Igorevitch Ianov (Student Member) received his B.E. degree

in Engineering Systems and M.S. degree in Intelligent Information Systems from University of Tsukuba, Cybernics Laboratory, Japan. Currently he is continuing his research as a Ph.D. student in the same institution. He is a member of the Institute of Electrical Engineers of Japan (IEEJ), the Institute of Complex Medical Engineering (ICME) and the Institute of Electrical and Electronics Engineers (IEEE).

Hiroaki Kawamoto (Non-member) received his BE, ME and PhD from the University of Tsukuba, Japan in 1998, 2000 and 2004, respectively. Currently he is an Assistant Professor at Faculty of Engineering, Information and Systems, University of Tsukuba. His research interests include biomechanics, biorobotics and human-machine interfaces, in particular exoskeleton type robots. He is a member of the Robotics Society of Japan, and the Japan Society of Mechanical Engineers.

Yoshiyuki Sankai (Non-member) received his Ph.D. degree in engineering from the University of Tsukuba, Japan in 1987. He was a Japan Society for the Promotion of Science Research Fellow, an Assistant Professor, an Associate Professor and a Professor in the Institute of Systems and Engineering, University of Tsukuba, and a Visiting Professor at Baylor College of Medicine, Houston, Texas, in the United States of America. He is currently a Professor of the Graduate School in Systems and Information Engineering, the Director of the Center for Cybernics Research, University of Tsukuba, the President/CEO of CYBERDYNE Inc. and the Leader of "FIRST" (Funding Program for World Leading Innovative R&D on Science and Technology) on Cybernics, funded by the Cabinet office of Japan. He was also the President of the Japan Society of Embolus Detection and Treatment, an Executive Board Member of the International Journal of the Robotics Society of Japan (RSJ), and the Chairman and a member of the Awards Committee of the RSJ, also an executive editor of Vascular Lab. He has won the World Technology Award (2005), the METI (Minister of Economy, Trade and Industry of Japan) Minister Award (2007) and other awards.